Supplementary Information

Pendant-Cation Assisted Spontaneous Axial Halide Substitution in Group 7 M(L)(CO)$_3$X Complexes

Wesley W. Kramer,* Thomas R. Sheridan, Jorge Pérez-Vázquez, Christophe A. Boivin, Amanda M. Browne, Catherine G. Logan, Brian C. Sanders

Table of Contents

Experimental Methods

General Information. All reagents and chemicals were purchased from Sigma-Aldrich, Alfa Aesar, or Strem Chemicals and used without further purification. Anhydrous solvents acetonitrile (MeCN), dimethylformamide (DMF), and dimethylsulfoxide (DMSO) were purchased from Sigma and used without further purification.

Physical Methods. ^{1}H and ^{13}C NMR spectra were recorded in the listed deuterated solvent with either a 300 MHz Bruker BZH 400/52, or 500 MHz Bruker Avance Neo Ascend 500 NMR spectrometer held at 298 K unless stated otherwise. All experimental data were collected with the sample rotating at 20 Hz. Chemical shifts are referenced to the residual protio signal of the deuterated solvent as previously reported.[1] FTIR-ATR Infrared spectra were recorded on a Nicolet Magna 860 FTIR or a Perkin-Elmer Spectrum Two. Solution phase FTIR spectra were recorded in an N_2 atmosphere glovebox on an Thermo Scientific Nicolet iS5 FTIR spectrometer. Electronic absorption spectra were collected on an Agilent 8453 or Cary 60 UV-vis spectrometer.

Electrochemical Methods

Electrochemical measurements were performed using a either a Biologic SP-200, or Pine WaveDriver 200 Potentiostat, 3 mm glassy carbon working electrodes, and a graphite rod (99.999% Strem Chemical) counter electrode. For non-aqueous electrochemical experiments potentials were measured versus a 1 mM $Ag/AgNO_3$ quasi-reference electrode (BASI) and are reported versus the ferrocenium/ferrocene ($Fc^{+/0}$) redox couple. In aqueous solution potentials are reported versus a saturated calomel electrode (SCE) reference.

Equilibrium Calculations

The equilibrium constants for the halide substitution reactions were determined according to the general equilibrium expression

$$K_{eq} = \frac{[M\text{–Solv}^+][Z^-]}{[M]}$$

Where [**M**], M = **1** or **2**, and [**M-Solv**$^+$], Solv = MeCN or H_2O are the sum of the normalized peak areas for the aromatic protons the respective complex divided by the number of protons represented by each peak (two protons per peak included in the sum). The concentration of the liberated axial halide (Z^- = Cl^- or Br^-) is assumed to be $[Z^-] = [\text{M-Solv}^+]$. The average normalized peak areas for the complexes were calculated from the "Absolute" peak area produced by the NMR analysis software MestReNova. For most complexes in this study the peaks of the parent complex were well separated from the peaks of the solvato complex as shown in Figure S3a. In those cases, an average of all three aromatic resonances of each species was used to calculate the average peak area. However, in the case of **1**|**PF$_6$** only the 6,6` protons can be integrated separately. For **2**|**Br** the 5,5` peak was excluded from the calculation because of overlapping peaks.

Table S1. Average Normalized peak areas of aromatic protons of **1|X** and **2|X** complexes and their corresponding solvato complexes under various conditions.

	Peak area, halide complex	Peak area, solvato complex
1|PF$_6$	2.00±0.00	0.058±0.001
1|PF$_6$, "wet"	2.00±0.00	0.077±0.007
1|PF$_6$ + 10 eq. $TBAPF_6$	2.00±0.00	0.141±0.014
1|PF$_6$ + 10 eq NH_4PF_6	2.00±0.00	0.583±0.015
1|Cl	0.882±0.099	1.989±0.056
2|PF6	1.98±0.10	0.379±0.143
2|PF$_6$, "wet"	1.99±0.05	0.753±0.024
2|PF$_6$ + 10 eq. $TBAPF_6$	1.97±0.06	0.800±0.039
2|Cl	0.167±0.016	2.03±0.08
2|Br	0.138±0.012	1.99±0.02

Synthesis of Compounds:

Scheme S1. Synthesis of tmam ligand.

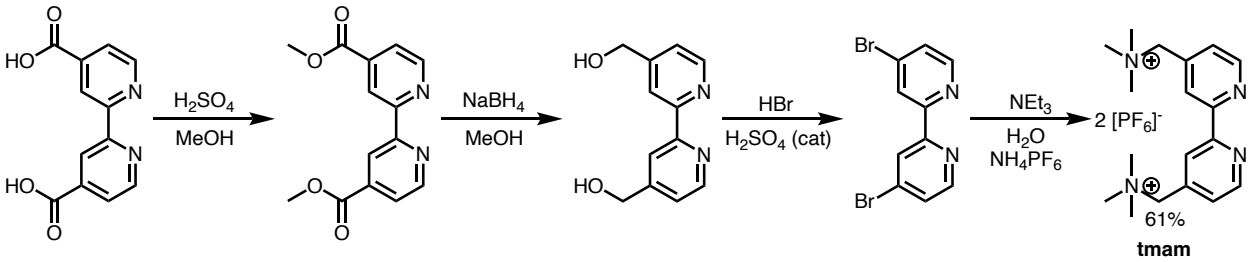

4,4′-bis[(trimethylamino)-methyl]-2,2′-bipyridine ($tmam^{2+}$). The PF_6^- salts of $tmam^{2+}$ were prepared as previously described in 61% yield over 4 steps.[2-4]

[Re^{I}(tmam)(CO)$_3$(Cl)](PF$_6$)$_2$ (1|PF$_6$). To a 10 mL acetone solution containing 0.300 g (0.508 mmol) $[tmam](PF_6)_2$ was added a 5 mL acetone solution containing 0.221 g (0.610 mmol) of $Re(CO)_5Cl$. The reaction mixture was sparged with N_2 and refluxed at 70 °C for 16 h. After cooling to RT, the heterogeneous yellow solution mixture was stirred and cooled with an ice bath. Addition of 20 mL of EtOH precipitated the remaining material as a yellow solid. The solid material was collected by filtration with a medium glass fritted funnel then washed with EtOH (3 × 20 mL portions) followed by washing with Et_2O (3 × 20 mL portions). The yellow solid was collected and dried under reduced pressure overnight to afford 0.390 g, 0.435 mmol, 86%. X-ray diffraction quality crystals were grown from diffusion of Et_2O into an MeCN solution of **1|PF$_6$**, in the absence of light at RT overnight. ^{1}H NMR (500 MHz, DMSO) δ 9.22 (d, J = 5.6 Hz, 2H), 8.74 (s, 2H), 7.93 (dd, J = 5.6, 1.7 Hz, 2H), 4.85 – 4.63 (m, 4H), 3.18 (s, 18H). FTIR (ATR), ν_{max} (cm^{-1}): 2018(vs, ν_{CO}), 1919 (vs, ν_{CO}), 1891 (vs, ν_{CO}), 822 (vs, ν_{PF}). UV-vis (DMSO, 298 K), λ_{max}, nm (ε, M^{-1} cm^{-1}): 390 (**14,000**); 456 (3,800). Anal. Calcd for $C_{21}H_{28}ClN_4O_3ReF_{12}P_2$: C, 28.15; H, 3.15; N, 6.25. Found: C, 28.72; H, 3.29; N, 6.64.

[Re(tmam)(CO)$_3$(MeCN)](PF$_6$)$_3$ (1-MeCN$^+$). **1-MeCN$^+$** was prepared by addition of 42.3 mg (0.167 mmol) $AgPF_6$ to an MeCN solution of **1|PF$_6$** (150 mg, 0.167 mmol**)**. The reaction was protected from light with an aluminum foil jacket and stirred at reflux overnight. The AgCl precipitate was removed by filtration of the reaction mixture through a bed of celite. The filtrate was concentrated under vacuum and the product was precipitated by addition of Et_2O. The product was isolated as a yellow solid in quantitative yield (152.4 mg). ^{1}H NMR (500 MHz, CD_3CN) δ 9.17 (d, *J* = 5.6 Hz, 2H), 8.59 (d, *J* = 1.8 Hz, 2H), 7.85 (dd, *J* = 5.7, 1.7 Hz, 2H), 4.61 (d, *J* = 1.5 Hz, 4H), 3.17 (s, 18H). FTIR (ATR), ν_{max} (cm^{-1}): 2039(vs, ν_{CO}), 1937 (br, ν_{CO}), 823 (vs, ν_{PF}) UV-vis (MeCN, 298 K) λ_{max}, nm (ε, M^{-1} cm^{-1}) 249 (18000), 284 (15000), 312 (13000), 326 (13000), 359 (4300)

[Re(tmam)(CO)$_3$(Cl)](Cl)$_2$ (1|Cl). To a 50 mL acetone solution containing 1.00 g (1.693 mmol) of tmam-PF_6 was added a 10 mL acetone solution containing 0.704 g (1.95 mmol) of $Re(CO)_5Cl$. The reaction mixture was sparged with N_2 and refluxed for 16 h. After reflux, the small amount of insoluble material was dissolved with additional acetone providing a bright, homogenous, yellow-orange colored solution. A saturated acetone solution of tetrabutylammonium chloride was added dropwise to precipitate a bright yellow solid that was then filtered and dried under vacuum. Excess tetrabutylammonium chloride was removed the bulk yellow solid by sonicating the product in acetone, the resulting slurry was then centrifuged at 5000 rpm for 10 minutes. The acetone was decanted and the solid was resuspended and the washing process was repeated three times. After the final acetone wash the product was resuspended in diethyl ether. The slurry was filtered and the solid was dried under reduced pressure overnight afforded the desired product (0.8900 g, 1.507 mmol, 92%). ^{1}H NMR (500 MHz, DMSO) δ 9.54 (d, *J* = 1.9 Hz, 2H), 9.19 (d, *J* = 5.6 Hz, 2H), 7.93 (dd, *J* = 5.7, 1.7 Hz, 2H), 4.85 (d, *J* = 20.8 Hz, 4H), 3.24 (s, 18H). FTIR (ATR), ν_{max} (cm^{-1}): 2023(vs, ν_{CO}), 1910 (vs, ν_{CO}), 1837 (vs, ν_{CO}). UV-vis (DMSO, 298 K) λ_{max}, nm (ε, M^{-1} cm^{-1}): 303 (16,000), 390 (3400). Anal. Calcd for $C_{21}H_{28}Cl_3N_4O_3Re$: C, 37.26; H, 4.17; N, 8.28. Found: C, 35.30; H, 4.41; N, 8.06

[Mn^I(tmam)(CO)$_3$(Br)](PF$_6$)$_2$ (2|PF$_6$). All Mn reactions were performed in minimal light or under red light. Compound **2|PF$_6$** was prepared analogously to **1|PF$_6$** with 0.300 g (0.508 mmol) of tmam-PF_6 and 0.345 g (0.610 mmol) of $Mn(CO)_5Br$ to afford a bright yellow-orange powder (0.345 g, 0.426 mmol, 84%). ^{1}H NMR (500 MHz, DMSO) δ 9.40 (d, *J* = 5.6 Hz, 2H), 8.65 (s, 2H), 7.90 (dd, *J* = 5.5, 1.7 Hz, 2H), 4.85 – 4.59 (m, 4H), 3.18 (s, 18H). FTIR (ATR), ν_{max} (cm^{-1}): 2023(vs, ν_{CO}), 1944 (vs, ν_{CO}), 1931 (vs, ν_{CO}), 1911 (vs, ν_{CO}), 824 (vs, ν_{PF}). UV-vis (DMSO, 298 K) λ_{max}, nm (ε, M^{-1} cm^{-1}): 305 (23,000), 437 (3400). Anal. Calcd for $C_{21}H_{28}BrN_4O_3MnF_{12}P_2$: C, 32.98; H, 3.69; N, 7.33. Found: C, 31.01; H, 3.57; N, 7.11.

[Mn(tmam)(CO)$_3$(MeCN)](PF$_6$)$_3$ (2-MeCN$^+$). The MeCN adduct of **2** was prepared by addition of 31.8 mg (0.126 mmol) $AgPF_6$ to an acetonitrile solution of **2|PF$_6$** (101.7 mn 0.126 mmol**)**. The reaction was allowed to stir at RT overnight in a vial . The AgBr precipitate was removed by filtration. The filtrate was concentrated under vacuum and the product was precipitated by addition of Et_2O. The product was isolated as a yellow solid (46.5 mg, 48% yield). ^{1}H NMR (500 MHz, CD_3CN) δ 9.28 (d, *J* = 5.6 Hz, 2H), 8.48 (s, 2H), 7.83 (d, *J* = 5.7 Hz, 2H), 4.59 (s, 4H), 3.16 (s, 18H). FTIR (ATR), ν_{max} (cm^{-1}): 2039(vs, ν_{CO}), 1937 (br, ν_{CO}), 821 (vs, ν_{PF}). UV-vis (MeCN, 298 K) λ_{max}, nm (ε, M^{-1} cm^{-1}) 246 (15000), 296 (20000), 389 (3700)

[Mn(tmam)(CO)$_3$(Br)](Cl)$_2$ (2|Cl). All Mn reactions were performed in minimal light or under red light. Compound **2|Cl** was prepared analogously to **1|Cl** with 1.00 g (1.69 mmol) of tmam-PF_6 and 0.536 g (1.95 mmol) of $Mn(CO)_5Br$. ^{1}H NMR (500 MHz, DMSO) δ 9.34 (d, *J* = 5.6 Hz, 2H), 9.27 (s, 2H), 7.90 (d, *J* = 5.6 Hz, 2H), 4.82 (d, *J* = 18.4 Hz, 4H), 3.22 (s, 19H). FTIR (ATR), ν_{max} (cm^{-1}): 2024(vs, ν_{CO}), 1934 (vs, ν_{CO}), 1931 (vs, ν_{CO}), 1911 (vs, ν_{CO}) λ_{max}, nm (ε, M^{-1} cm^{-1}): 305 (21,000), 433 (3200). Anal. Calcd for $C_{21}H_{28}BrN_4O_3MnCl_2$: C, 42.47; H, 4.78; N, 9.49. Found: C, 41.28; H, 5.28; N, 8.97.

[Mn(tmam)(CO)$_3$Br](Br)$_2$ (2|Br). All Mn reactions were performed in minimal light or under red light. Addition of 239.0 mg (0.741 mmol) TBABr to a solution of **2|PF$_6$** (75.0 mg, 0.0927 mmol) in 5 mL acetone resulted in the precipitation of **2|Br** as an orange solid. The suspension was stirred overnight at room temperature in an aluminum-jacketed scintillation vial then transferred to a centrifuge tube and centrifuged at 5000 rpm for 10 min. The acetone mother liquor was decanted then the product was resuspended in acetone and centrifuged again. This process was repeated three times to remove excess TBABr. After the final wash the product was suspended in Et_2O and collected over a frit. The product was isolated as a dark orange solid (25.4 mg, 40.5% yield). ^{1}H NMR (500 MHz, DMSO) δ 9.38 (d, J = 5.6 Hz, 2H), 9.11 (s, 2H), 7.90 (d, J = 5.7 Hz, 2H), 4.93 – 4.68 (m, 4H), 3.22 (s, 18H). FTIR (ATR), ν_{max} (cm^{-1}): 2023(vs, ν_{CO}), 1907 (br, ν_{CO}) UV-vis (DMSO, 298 K) λ_{max}, nm (ε, M^{-1} cm^{-1}): 305 (22,000), 433 (3300).

Structural Data

Low-temperature diffraction data (ϕ-and ω-scans) were collected on a Bruker AXS D8 VENTURE KAPPA diffractometer coupled to a PHOTON 100 CMOS detector with Mo K_α radiation (λ = 0.71073 Å) from an IμS micro-source for the structure of compound P17338. The structure was solved by direct methods using SHELXS[5] and refined against F^2 on all data by full-matrix least squares with SHELXL-2016[6] using established refinement techniques.[7] All non-hydrogen atoms were refined anisotropically. All hydrogen atoms were included into the model at geometrically calculated positions and refined using a riding model. The isotropic displacement parameters of all hydrogen atoms were fixed to 1.2 times the U value of the atoms they are linked to (1.5 times for methyl groups). All disordered atoms were refined with the help of similarity restraints on the 1,2- and 1,3-distances and displacement parameters as well as enhanced rigid bond restraints for anisotropic displacement parameters.

Compound [Re(tmam)(CO)$_3$(MeCN)](PF$_6$)$_3$ (**1-MeCN$^+$**) crystallizes in the triclinic space group P-1 with one molecule in the asymmetric unit along with three PF_6^{1-} anions, half a molecule of acetonitrile and half a molecule of diethyl ether. The three PF_6^{1-} anions are located over four independent positions. Two of these PF_6^{1-} anions are located near crystallographic inversion centers and were disordered appropriately. The acetonitrile and diethyl ether are also located near a crystallographic inversion center and were disordered appropriately.

Compound [Mn(tmam)(CO)$_3$(Br)](PF$_6$)$_2$ (**2|PF$_6$**) crystallizes in the monoclinic space group $P2_1/c$ with one molecule in the asymmetric unit. The structure was modeled with 0.3 molecules of water in the asymmetric unit. The hydrogen atoms for this partially occupied water could not be located and were not included in the model.

Compound [Re(tmam)(CO)$_3$(Cl)](PF$_6$)$_2$ (**1|PF$_6$**) crystallizes in the monoclinic space group $P2_1/c$ with one molecule in the asymmetric unit along with half a molecule of acetonitrile. The acetonitrile is located near a crystallographic inversion center and was disordered over two positions.

Table S2. Crystal data and structure refinement for for [Re(tmam)(CO)$_3$(MeCN)](PF$_6$)$_3$ (**1-MeCN$^+$**).

Empirical formula	$C_{28}H_{40.50}F_{18}N_{6.50}O_{3.50}P_3Re$	
Formula weight	1145.28	
Temperature	100(2) K	
Wavelength	0.71073 Å	
Crystal system	Triclinic	
Space group	P-1	
Unit cell dimensions	a = 13.0356(6) Å	a= 113.8926(17)°.
b = 13.2377(6) Å	b= 96.814(2)°.	
c = 14.7412(7) Å	g = 111.3674(18)°.	

Volume	2057.32(17) $Å^3$
Z	2
Density (calculated)	1.849 Mg/m^3
Absorption coefficient	3.193 mm^{-1}
F(000)	1128
Crystal size	0.350 x 0.250 x 0.100 mm^3
Theta range for data collection	2.243 to 36.384°.
Index ranges	-21<=h<=21, -22<=k<=22, -24<=l<=24
Reflections collected	60104
Independent reflections	19968 [R(int) = 0.0474]
Completeness to theta = 25.242°	99.8 %
Absorption correction	Semi-empirical from equivalents
Max. and min. transmission	0.7471 and 0.6088
Refinement method	Full-matrix least-squares on F^2
Data / restraints / parameters	19968 / 1498 / 773
Goodness-of-fit on F^2	1.031
Final R indices [I>2sigma(I)]	R1 = 0.0415, wR2 = 0.0665
R indices (all data)	R1 = 0.0644, wR2 = 0.0717
Extinction coefficient	n/a
Largest diff. peak and hole	1.432 and -1.097 $e.Å^{-3}$

Table S3. Crystal data and structure refinement for $[Mn(tmam)(CO)_3(Br)](PF_6)_2$ (**2**|**PF_6**).

Empirical formula	$C_{21}H_{28.67}BrF_{12}MnN_4O_{3.33}P_2$
Formula weight	815.26
Temperature	100(2) K
Wavelength	1.54178 Å
Crystal system	Monoclinic
Space group	$P2_1/c$
Unit cell dimensions	a = 18.0875(14) Å a= 90°.
b = 13.3416(11) Å	b= 94.982(5)°.
c = 12.7322(9) Å	g = 90°.
Volume	3060.9(4) $Å^3$
Z	4
Density (calculated)	1.769 Mg/m^3
Absorption coefficient	7.024 mm^{-1}
F(000)	1629
Crystal size	0.100 x 0.050 x 0.050 mm^3
Theta range for data collection	2.452 to 73.496°.
Index ranges	-22<=h<=21, -16<=k<=16, -15<=l<=15
Reflections collected	29184
Independent reflections	6147 [R(int) = 0.1328]
Completeness to theta = 67.679°	100.0 %
Absorption correction	Semi-empirical from equivalents

Max. and min. transmission	0.7538 and 0.6132
Refinement method	Full-matrix least-squares on F^2
Data / restraints / parameters	6147 / 0 / 412
Goodness-of-fit on F^2	1.019
Final R indices [I>2sigma(I)]	R1 = 0.0783, wR2 = 0.1650
R indices (all data)	R1 = 0.1261, wR2 = 0.1913
Extinction coefficient	n/a
Largest diff. peak and hole	0.666 and -0.929 e.Å^{-3}

Table S4. Crystal data and structure refinement for for $[Re(tmam)(CO)_3(Cl)](PF_6)_2$ (**1**|**PF$_6$**).

Empirical formula	$C_{22}H_{29.50}ClF_{12}N_{4.50}O_3P_2Re$	
Formula weight	916.59	
Temperature	100(2) K	
Wavelength	0.71073 Å	
Crystal system	Monoclinic	
Space group	$P2_1/c$	
Unit cell dimensions	a = 18.1497(10) Å	□= 90°.
	b = 13.5754(9) Å	□= 96.113(3)°.
	c = 12.6756(8) Å	□ = 90°.
Volume	3105.4(3) Å^3	
Z	4	
Density (calculated)	1.961 Mg/m^3	
Absorption coefficient	4.209 mm^{-1}	
F(000)	1788	
Crystal size	0.100 x 0.100 x 0.050 mm^3	
Theta range for data collection	2.257 to 36.321°.	
Index ranges	-23<=h<=30, -22<=k<=15, -21<=l<=21	
Reflections collected	42554	
Independent reflections	14868 [R(int) = 0.0384]	
Completeness to theta = 25.242°	99.8 %	
Absorption correction	Semi-empirical from equivalents	
Max. and min. transmission	0.7471 and 0.6427	
Refinement method	Full-matrix least-squares on F^2	
Data / restraints / parameters	14868 / 0 / 431	
Goodness-of-fit on F^2	1.037	
Final R indices [I>2sigma(I)]	R1 = 0.0442, wR2 = 0.0897	
R indices (all data)	R1 = 0.0700, wR2 = 0.1007	
Extinction coefficient	n/a	
Largest diff. peak and hole	4.880 and -2.659 e.Å^{-3}	

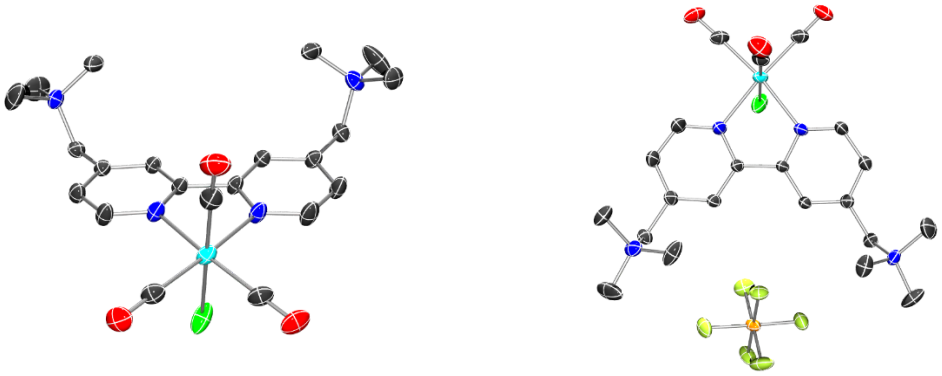

Figure S1. ORTEP of the dication of $[Re(tmam)(CO)_3(Cl)](PF_6)_2$ (**1**|**PF$_6$**) (50% thermal probability for all non-hydrogen atoms). (*Right*) Alternative view showing the PF_6^- in the cationic pocket. MeCN solvent of crystallization has been omitted for clarity.

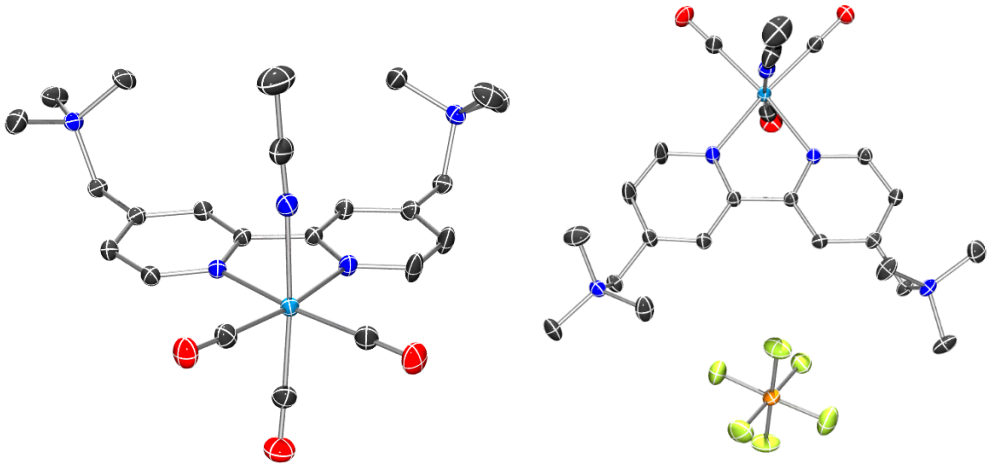

Figure S2. ORTEP of the trication of $[Re(tmam)(CO)_3(MeCN)](PF_6)_3$ (**1-MeCN**) (50% thermal probability for all non-hydrogen atoms). (*Right*) Alternative view showing the PF_6^- in the cationic pocket. MeCN and Et_2O solvent of crystallization have been omitted for clarity.

Table S4. Selected bond distances (Å) and bond angles (deg) for $[Re(tmam)(CO)_3(Cl)](PF_6)_2$ (**1**|**PF$_6$**)

	Distances (Å)		**Angles (°)**
Re(1)-C(1)	1.945	C(1)-Re(1)-Cl(1)	176.4
Re(1)-C(2)	1.911	C(2)-Re(1)-N(1)	171.4
Re(1)-C(3)	1.923	C(3)-Re(1)-N(2)	174.6
Re(1)-N(1)	2.179	N(1)-Re(1)-N(2)	75.2
Re(1)-N(2)	2.173	C(2)-Re(1)-N(2)	97.6

Re(1)-Cl(1)	2.487	C(3)-Re(1)-N(1)	99.8
C(1)-O(1)	1.104	N(2)-Re(1)-Cl(1)	85.3
C(2)-O(2)	1.148	N(1)-Re(1)-Cl(1)	82.4
C(3)-O(3)	1.154	C(1)-Re(1)-C(2)	89.8
C(1)-N(3)	7.180	C(1)-Re(1)-C(3)	90.9
C(1)-N(4)	7.617	C(2)-Re(1)-C(3)	87.2

Table S5. Selected bond distances (Å) and bond angles (deg) for $[Mn(tmam)(CO)_3(Br)](PF_6)_2$ (**2|PF$_6$**)

	Distances (Å)		**Angles (°)**
Mn(1)-C(1)	1.829	C(1)-Mn(1)-Br(1)	179.0
Mn(1)-C(2)	1.844	C(2)-Mn(1)-N(1)	171.5
Mn(1)-C(3)	1.836	C(3)-Mn(1)-N(2)	176.0
Mn(1)-N(1)	2.054	N(1)-Mn(1)-N(2)	78.8
Mn(1)-N(2)	2.054	C(2)-Mn(1)-N(2)	95.2
Mn(1)-Br(1)	2.534	C(3)-Mn(1)-N(1)	98.0
C(1)-O(1)	1.115	N(2)-Mn(1)-Br(1)	89.7
C(2)-O(2)	1.049	N(1)-Mn(1)-Br(1)	85.4
C(3)-O(3)	1.107	C(1)-Mn(1)-C(2)	91.8
C(1)-N(3)	7.047	C(1)-Mn(1)-C(3)	91.4
C(1)-N(4)	7.397	C(2)-Mn(1)-C(3)	87.7

Table S6. Selected bond distances (Å) and bond angles (deg) for $[Re(tmam)(CO)_3(MeCN)](PF_6)_3$ (**1-MeCN$^+$**)

	Distances (Å)		**Angles (°)**
Re(1)-C(1)	1.922	C(1)-Re(1)-N(3)	175.8
Re(1)-C(2)	1.929	C(2)-Re(1)-N(1)	172.9
Re(1)-C(3)	1.923	C(3)-Re(1)-N(2)	172.2
Re(1)-N(1)	2.170	N(1)-Re(1)-N(2)	74.9
Re(1)-N(2)	2.175	C(2)-Re(1)-N(2)	98.1
Re(1)-N(3)	2.133	C(3)-Re(1)-N(1)	98.5
C(1)-O(1)	1.147	N(2)-Re(1)-N(3)	80.5
C(2)-O(2)	1.152	N(1)-Re(1)-N(3)	83.9
C(3)-O(3)	1.135	C(1)-Re(1)-C(2)	88.4

N(3)-N(4)	6.741	C(1)-Re(1)-C(3)	88.0
N(3)-N(5)	6.814	C(2)-Re(1)-C(3)	88.6

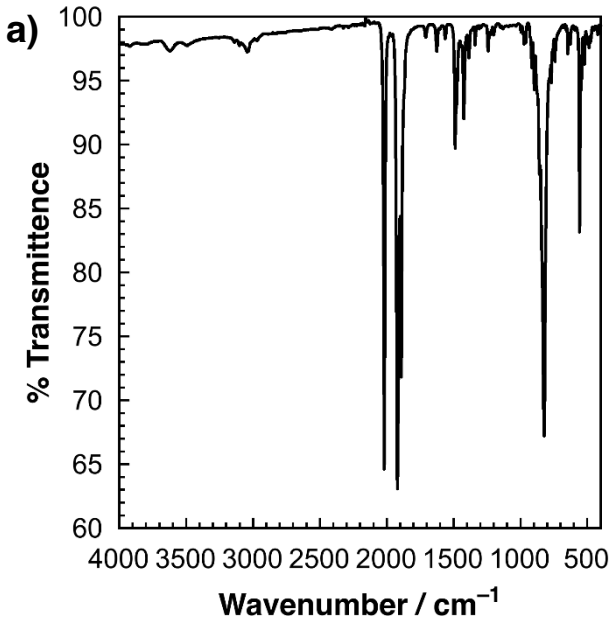

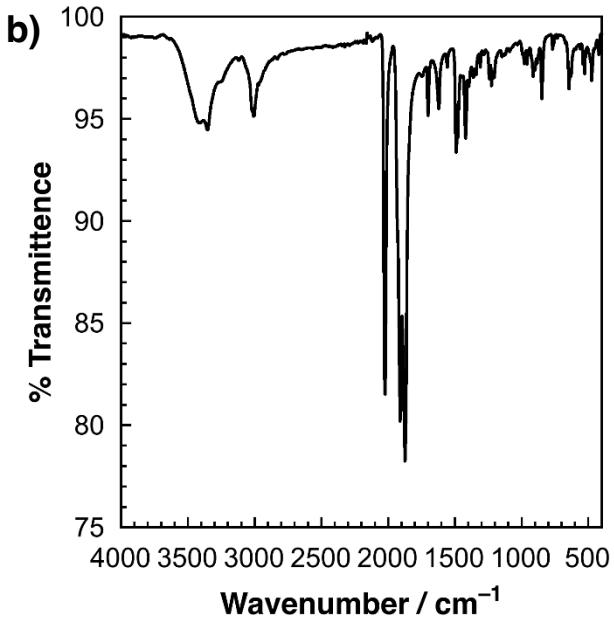

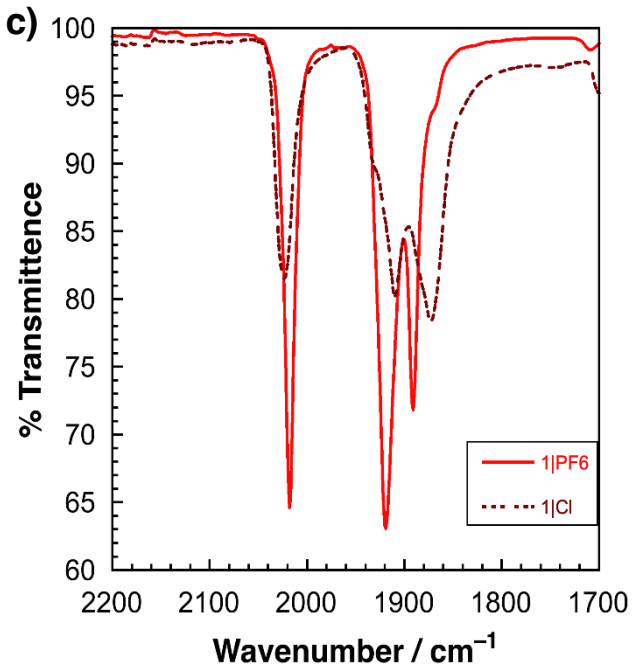

Figure S3: FT-IR vibrational spectra obtained from solid samples using an ATR module of **a) 1|PF$_6$, b) 1|Cl** and **c)** stacked spectra highlighting the CO peaks of **1|PF$_6$** and **1|Cl.**

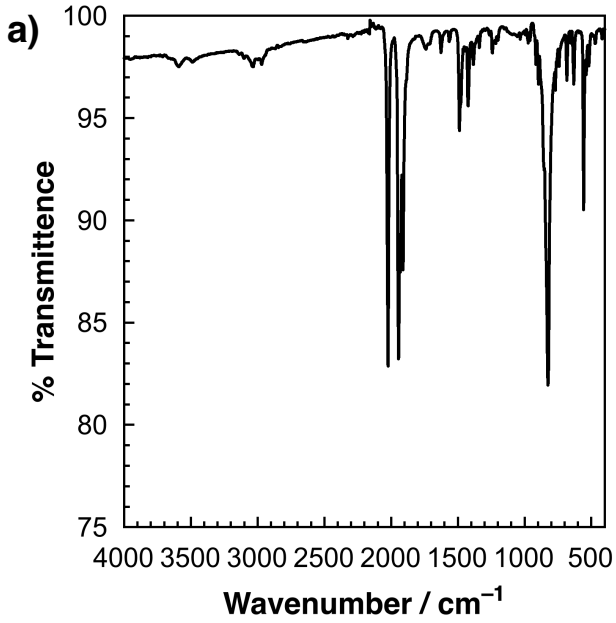

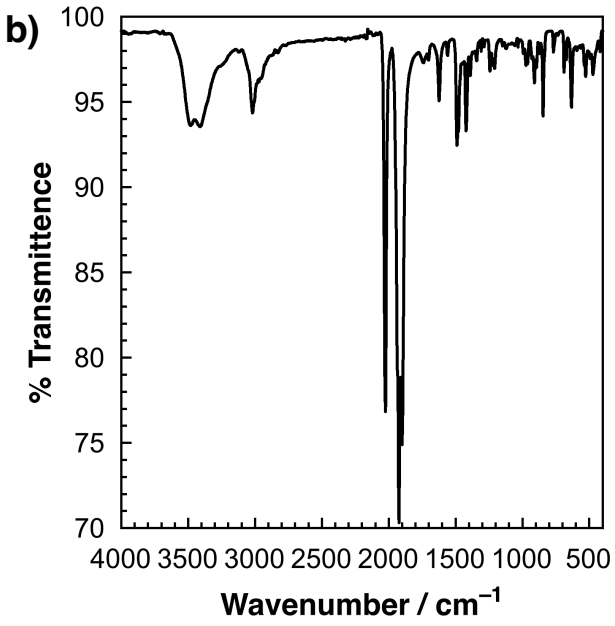
b)
100
95
90
85
80
75
70
% Transmittence
4000 3500 3000 2500 2000 1500 1000 500
Wavenumber / cm−1

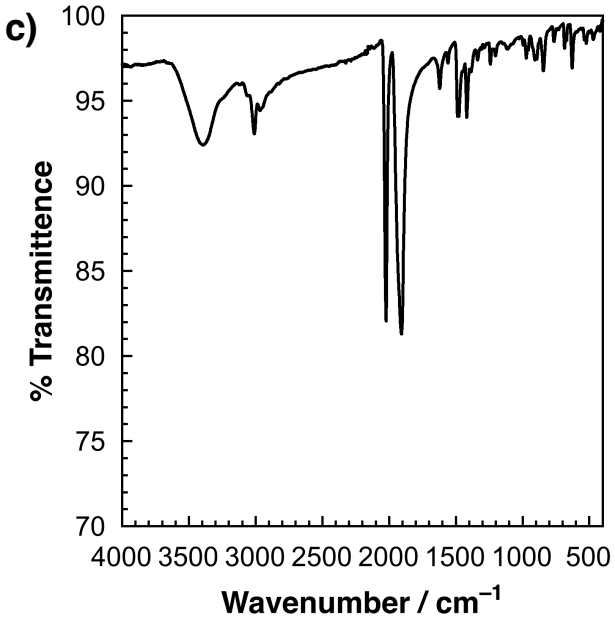
c)
100
95
90
85
80
75
70
% Transmittence
4000 3500 3000 2500 2000 1500 1000 500
Wavenumber / cm−1

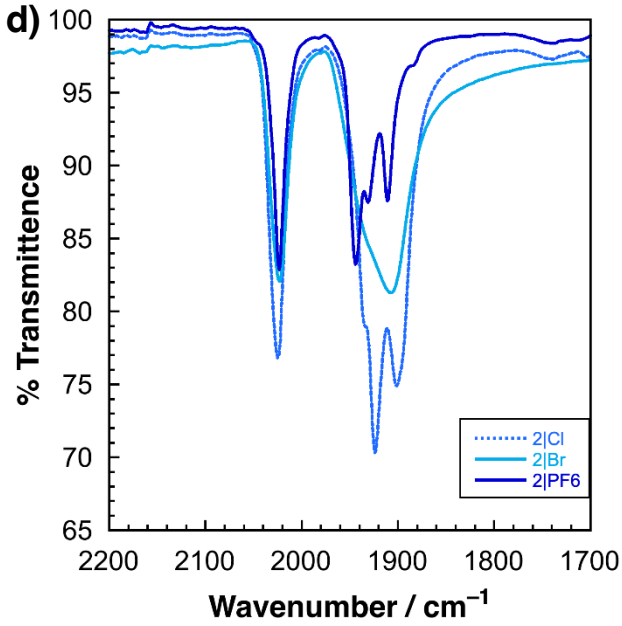

Figure S4: FT-IR vibrational spectra obtained from solid samples using an ATR module of **a) 2|PF$_6$**, **b) 2|Cl**, **c) 2|Br**, and **d)** stacked spectra highlighting the CO peaks of compounds **2|PF$_6$, 2|Cl** and **2|Br.**

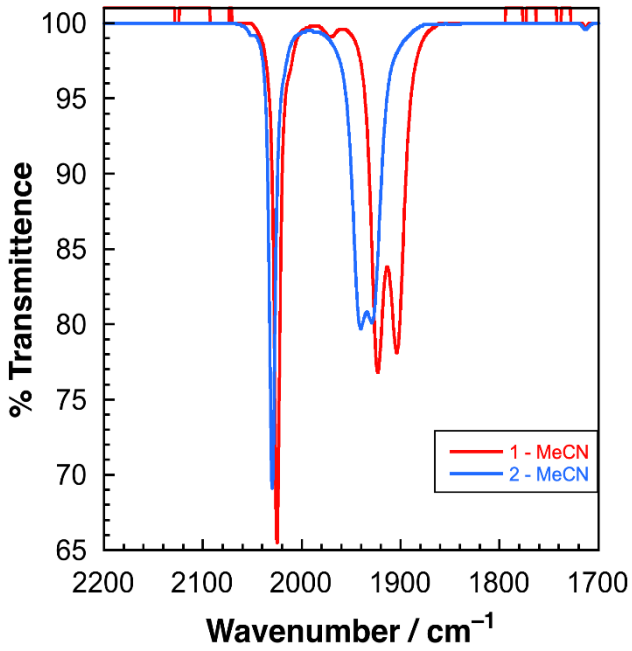

Figure S5: FT-IR vibrational spectra highlighting the CO peaks of compounds **1|PF$_6$** and **2|PF$_6$** in MeCN solution.

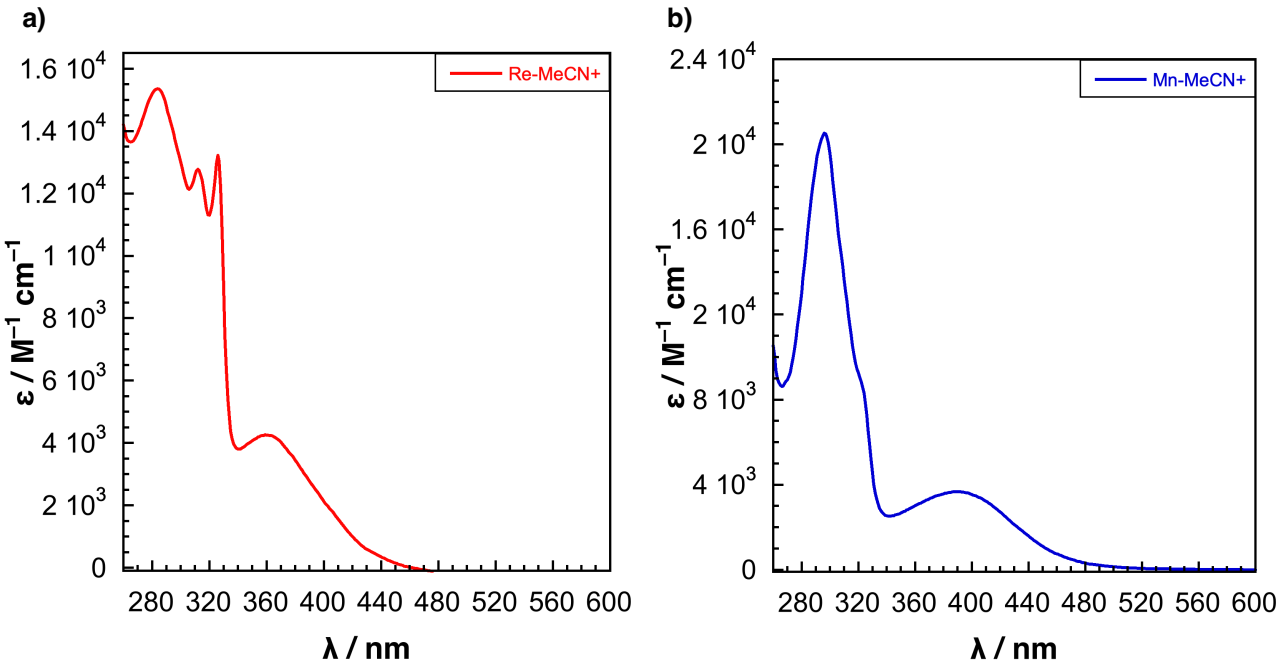

Figure S6. UV-vis spectra of **a) 1-MeCN**$^{+}$ and **b) 2-MeCN**$^{+}$ in MeCN. Molar absorptivity of each complex was calculated from a linear fit derived from absorbance spectra of each complex at 5 different concentrations.

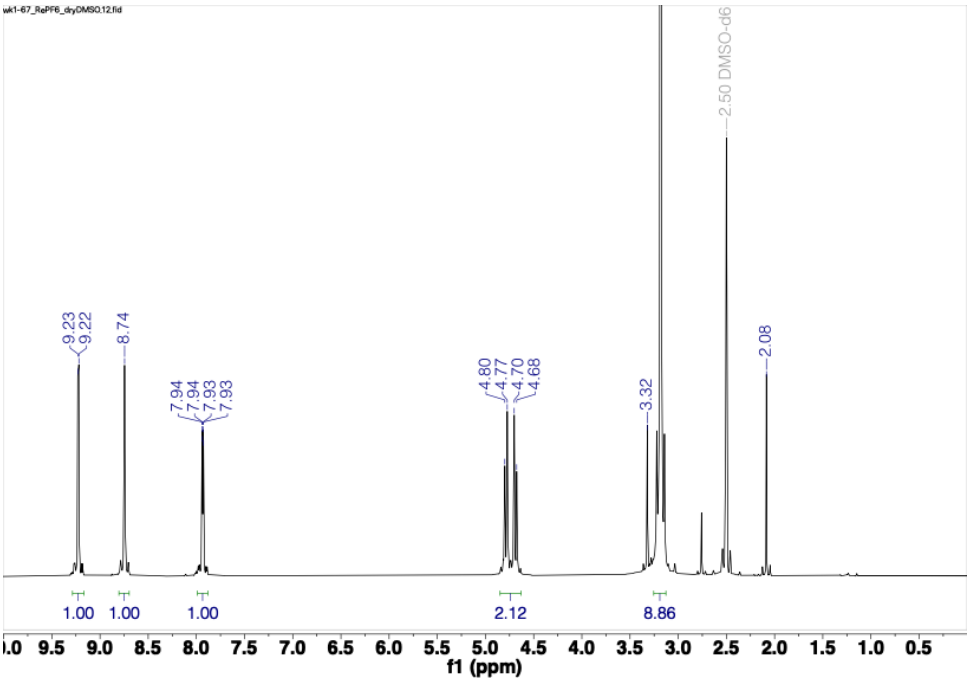

Figure S7. ^{1}H NMR spectrum of [Re(tmam)(CO)$_3$(Cl)](PF$_6$)$_2$ (**1**|**PF$_6$**) in DMSO-d_6

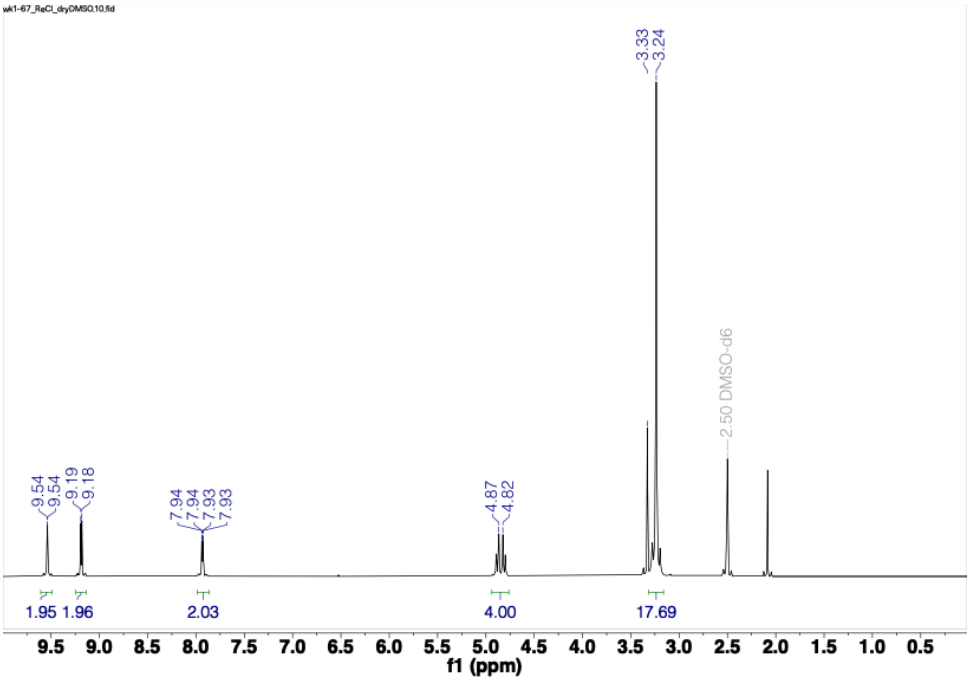

Figure S8. ^{1}H NMR spectrum of [Re(tmam)(CO)$_3$(Cl)](Cl)$_2$ (**1|Cl**) in DMSO-d_6.

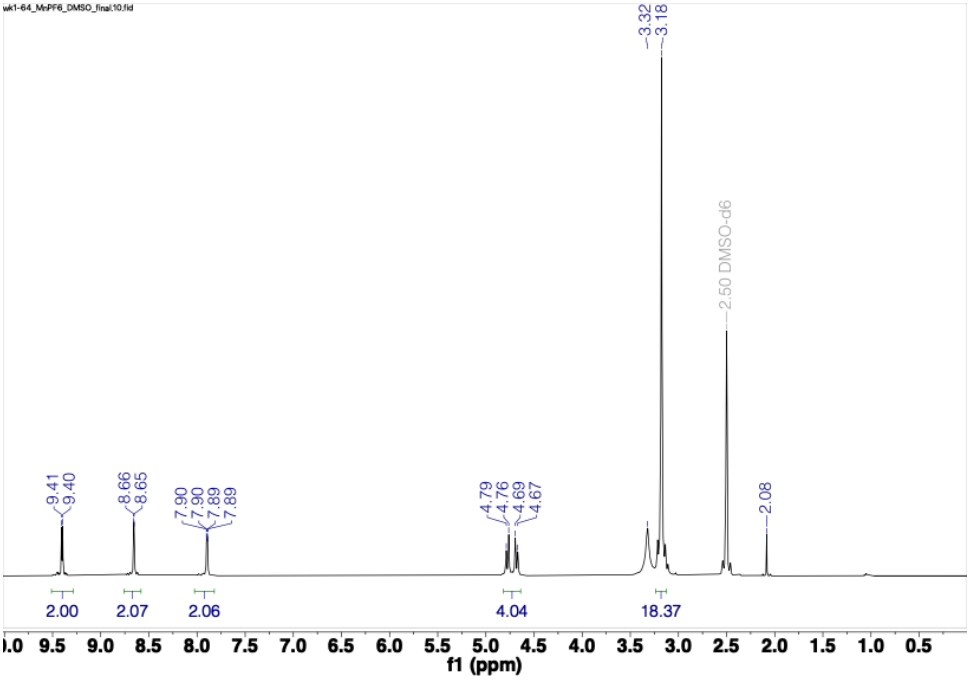

Figure S9. ^{1}H NMR spectrum of [Mn(tmam)(CO)$_3$(Br)](PF$_6$)$_2$ (**2|PF$_6$**) in DMSO-d_6.

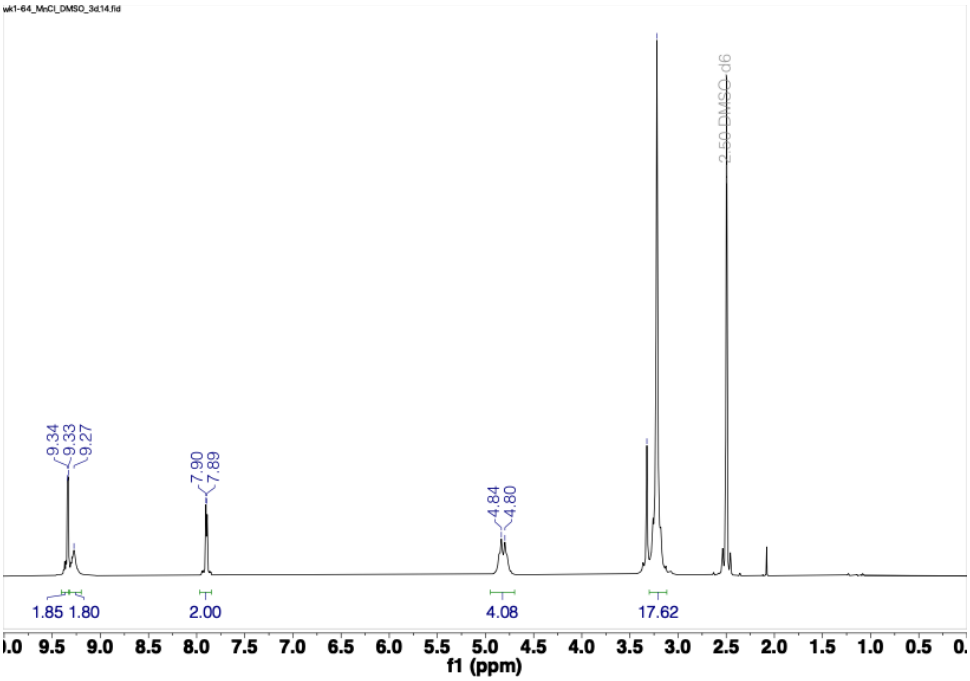

Figure S10. ^{1}H NMR spectrum of [Mn(tmam)(CO)$_3$(Br)](Cl)$_2$ (**2**|**Cl**) in DMSO-d_6.

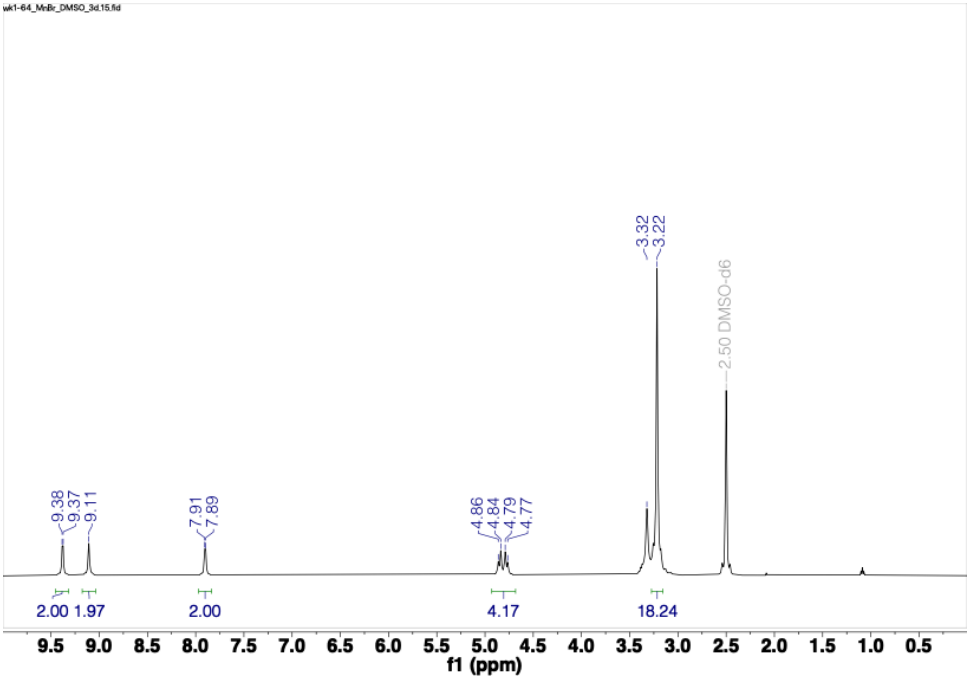

Figure S11. ^{1}H NMR spectrum of [Mn(tmam)(CO)$_3$(Br)](Br)$_2$ (**2**|**Br**) in DMSO-d_6.

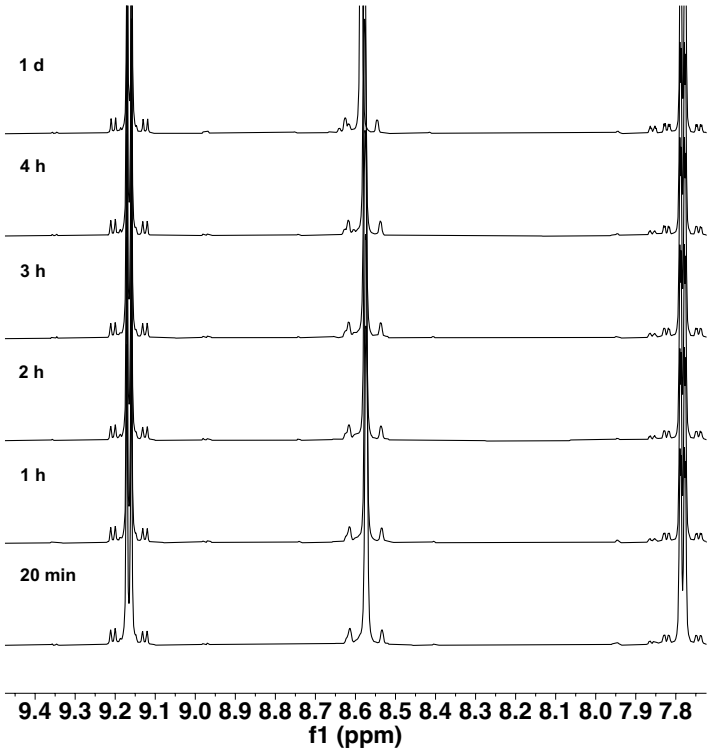

Figure S12. Evolution of the ^{1}H NMR spectrum of **1**|$\mathbf{PF_6}$ in MeCN-d_3 over the course of 1 d.

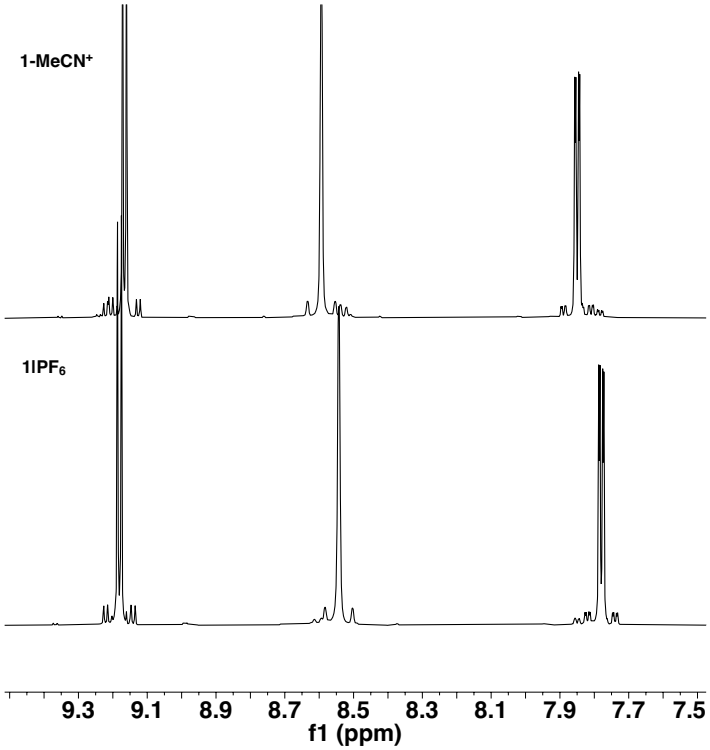

Figure S13. Comparison of the ^{1}H NMR spectra of **1**|$\mathbf{PF_6}$ and **1-MeCN**$^{+}$ in MeCN-d_3.

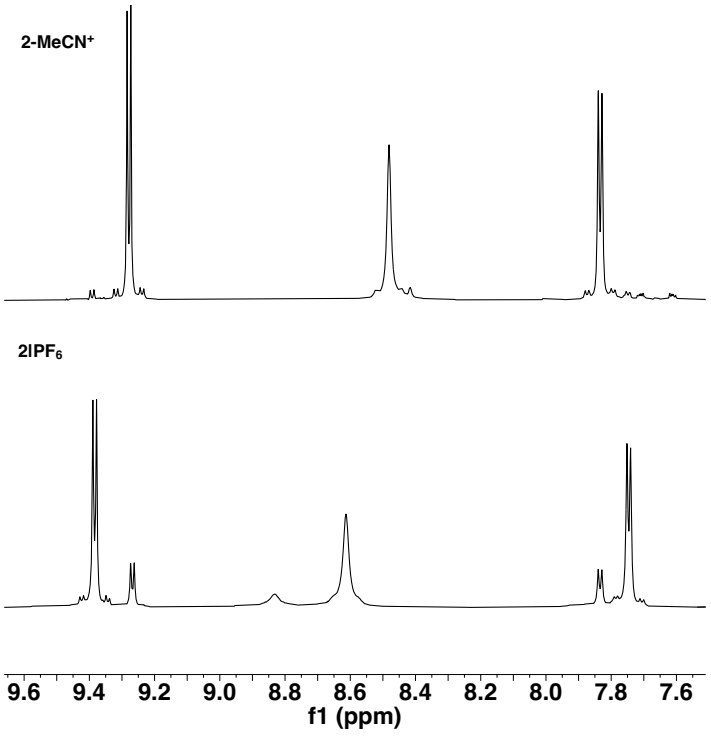

Figure S14. Comparison of the ^{1}H NMR spectra of **2**|$\mathbf{PF_6}$ and **2-MeCN**$^{+}$ in MeCN-d_3.

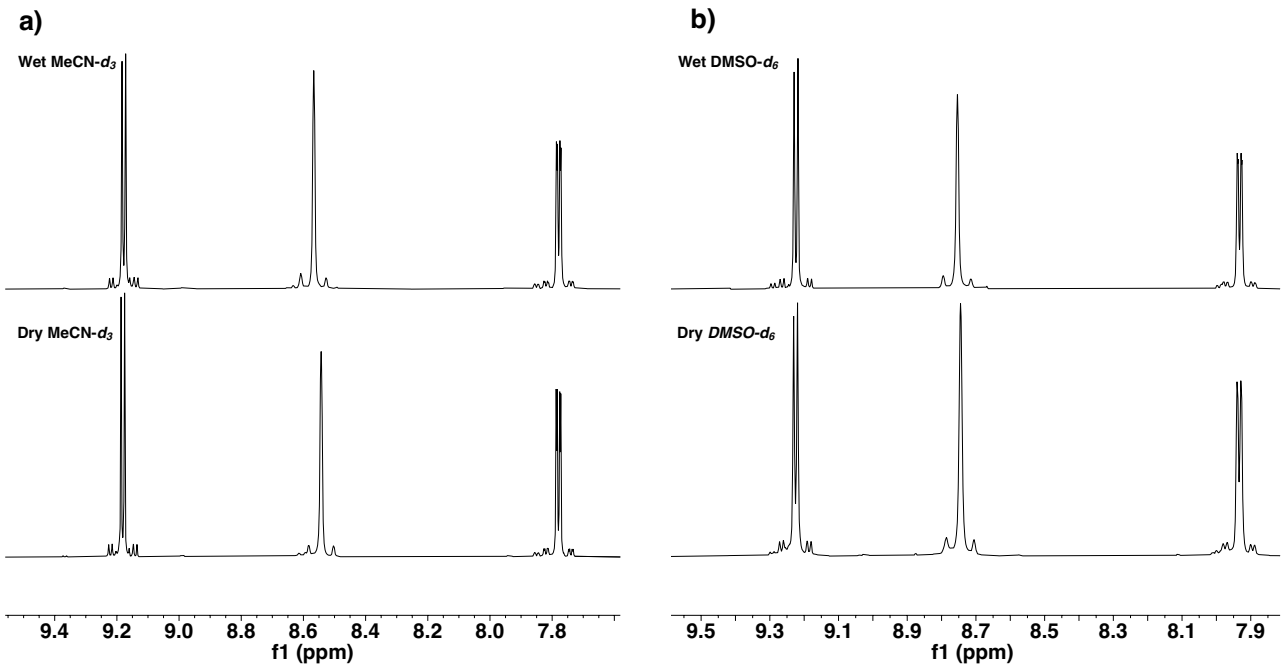

Figure S15. Comparison of ^{1}H NMR spectra of **1**|**PF$_6$** in wet and dry **a)** MeCN-d_3 and **b)** DMSO-d_6.

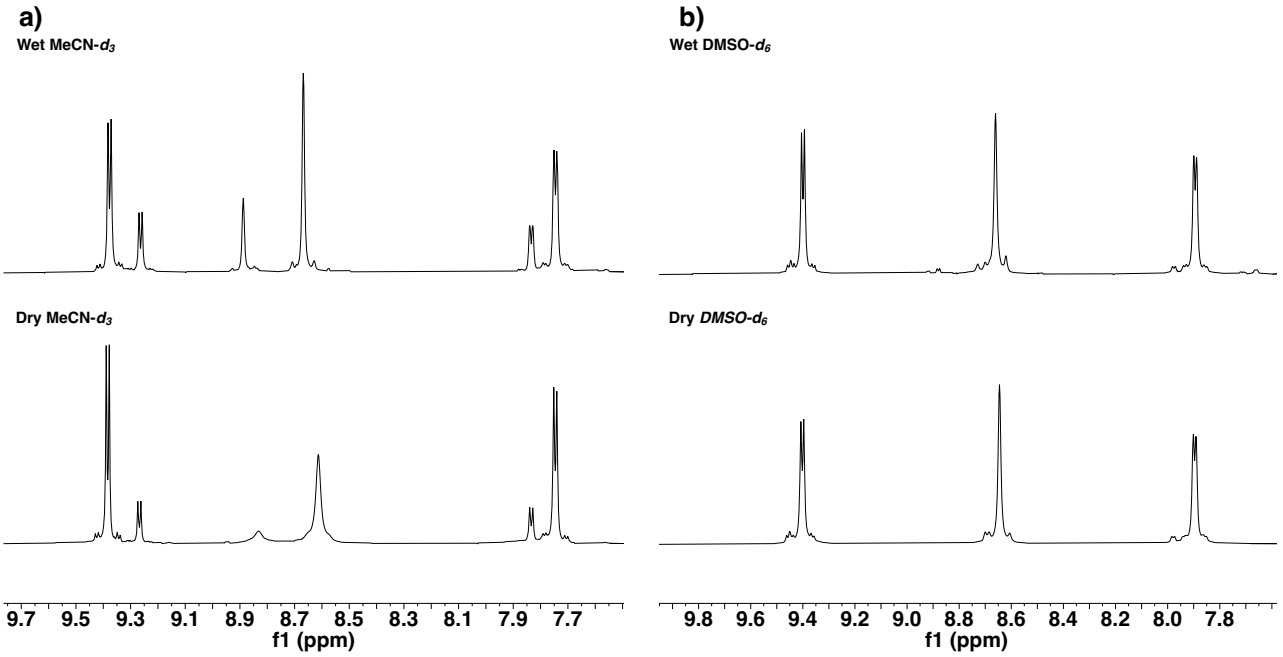

Figure S16. Comparison of ^{1}H NMR spectra of **2**|**PF$_6$** in wet and dry **a)** MeCN-d_3 and **b)** DMSO-d_6.

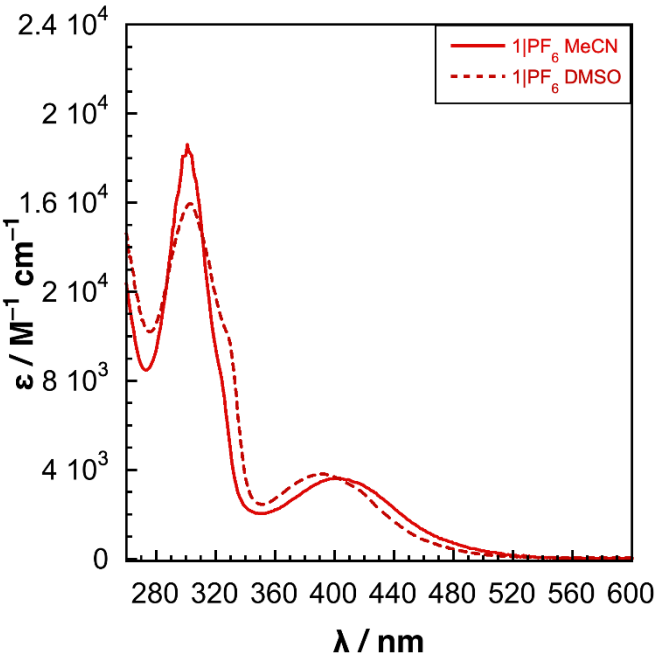

Figure S17. Comparison of the UV-vis speactrum of **1|PF$_6$** in MeCN and DMSO.

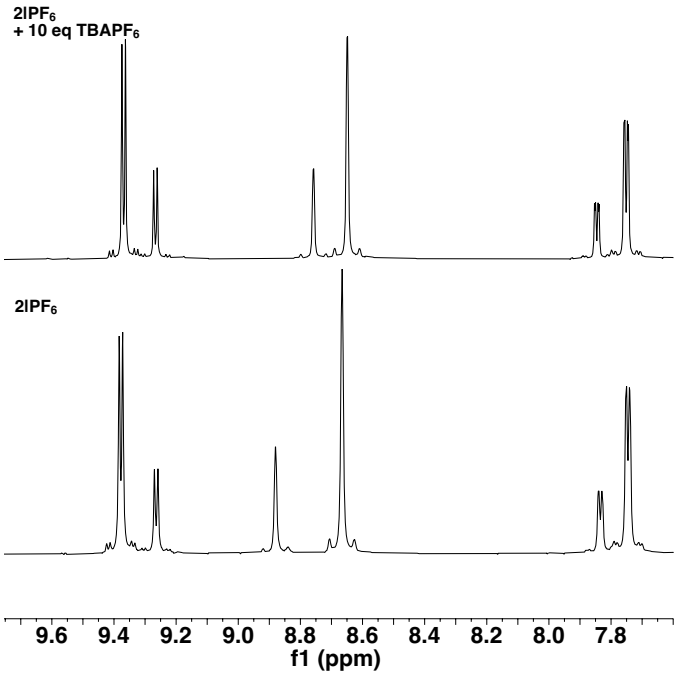

Figure S18. ^{1}H NMR spectrum of **2|PF$_6$ (10 mM)** in MeCN-d$_3$ with 0.1 M TBAPF$_6$ at equilibrium.

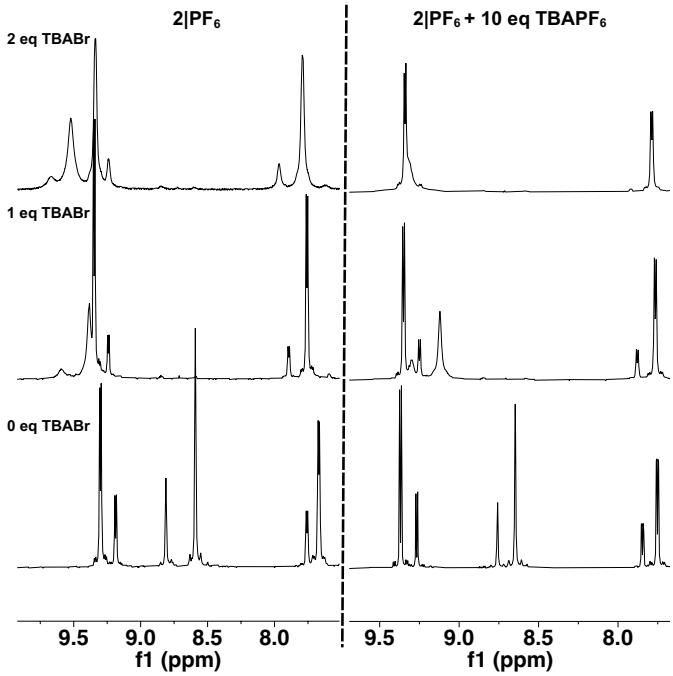

Figure S19. ^{1}H NMR spectra of **2|PF$_6$** showing the effect of TBABr additions on the equilibrium between **2** and **2-MeCN$^+$** with and without added TBAPF$_6$.

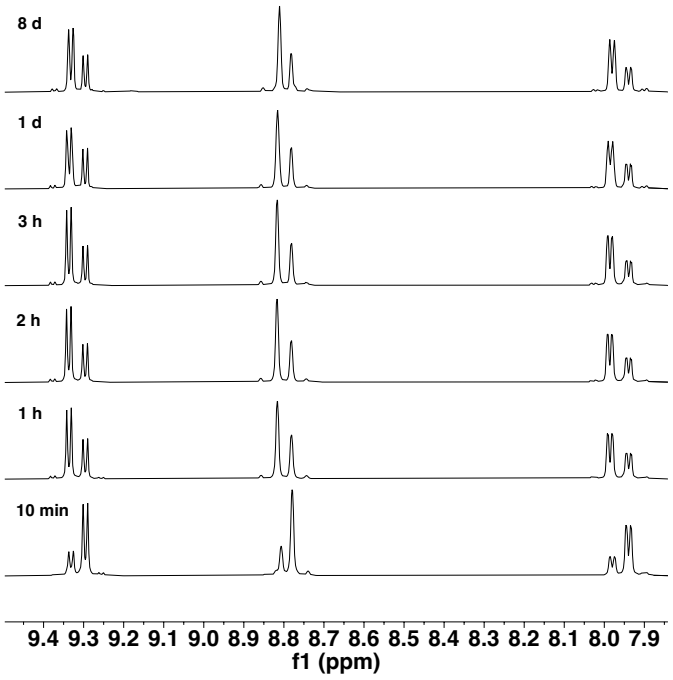

Figure S20. ^{1}H NMR spectrum of **1|Cl** in D_2O at several time points showing the system reaching equilibrium between **1** and **1-H$_2$O$^+$.**

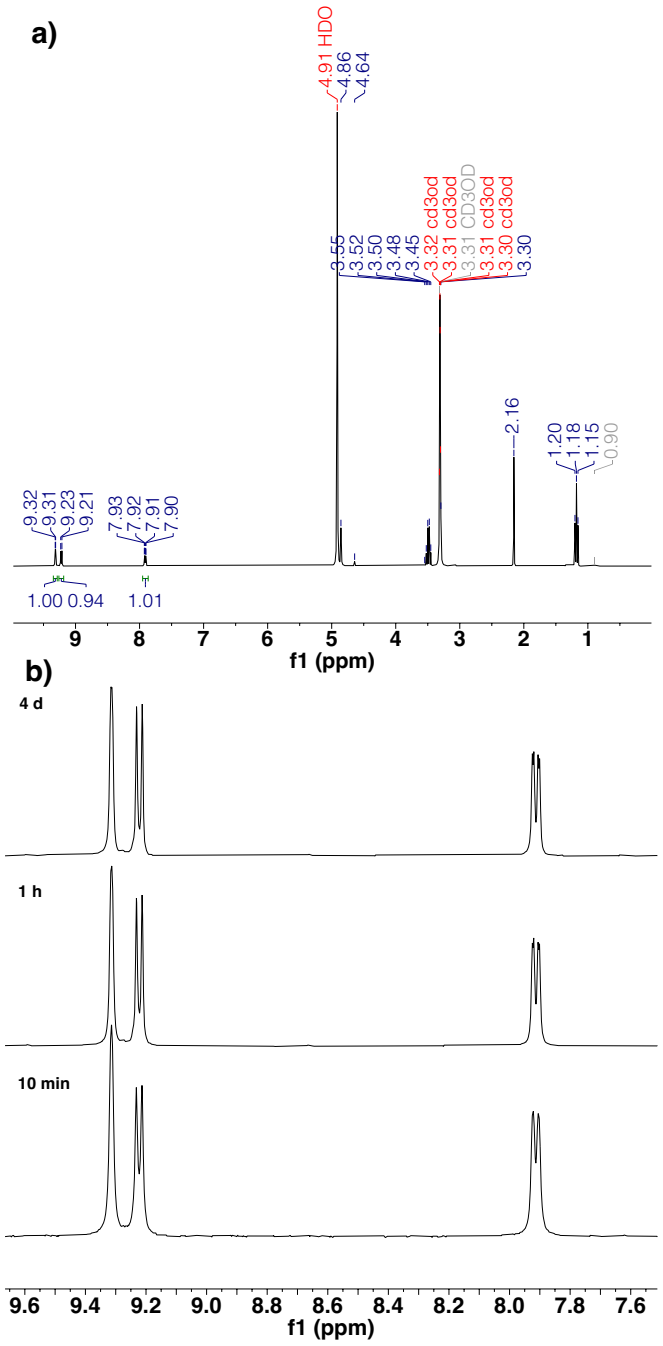

Figure S21. a) ^{1}H NMR spectrum of **1|Cl** in CD_3OD. b) ^{1}H NMR spectra of **1|Cl** in CD_3OD at 10 min, 1 h, and 4 d showing that halide substitution does not occur in methanol.

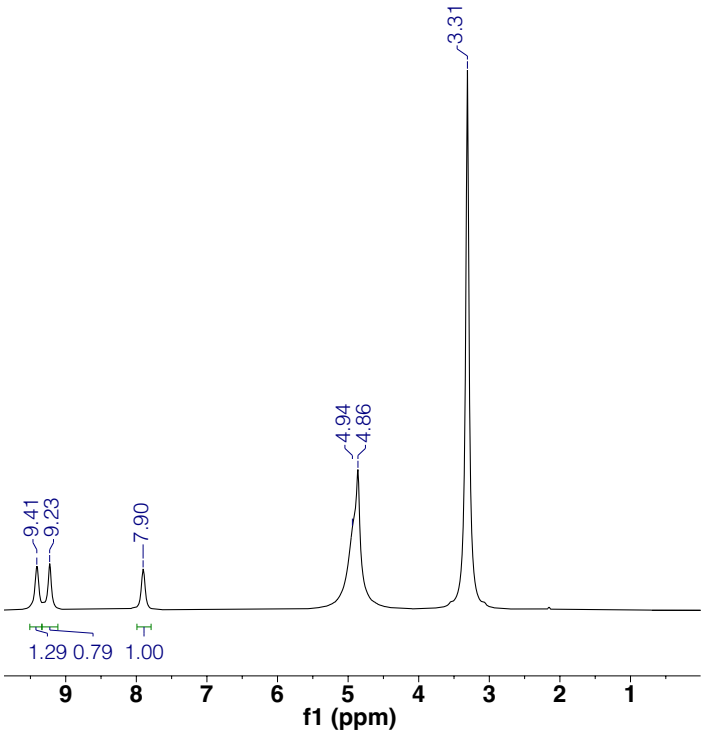

Figure S22. ^{1}H NMR spectrum of **2|Cl** in CD_3OD.

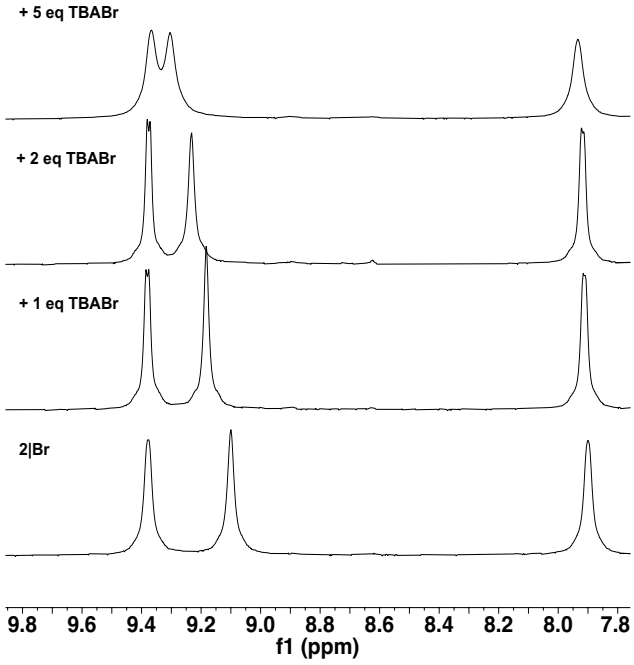

Figure S23. ^{1}H NMR spectra of **2|Br** in DMSO-d_6 showing the effect of added Br^-.

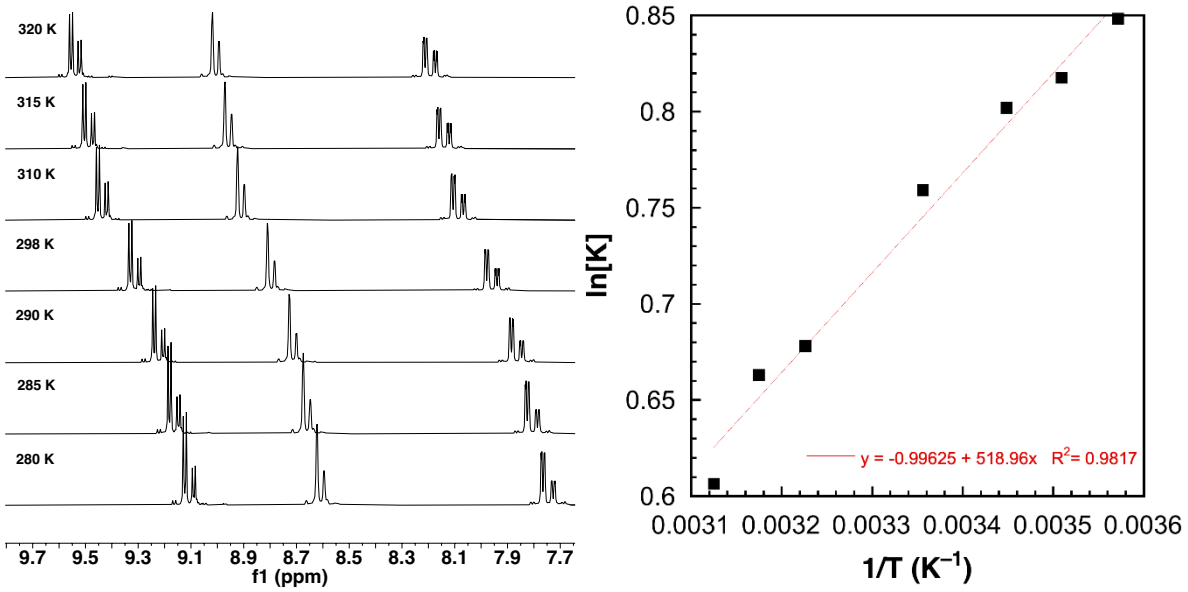

Figure S24. (*left*) ^{1}H NMR spectra of **1**|**Cl** at various temperatures (right) Van't Hoff plot constructed using the VT NMR data from the equilibrium concentrations of **1** and **1-H$_2$O$^+$** at various temperatures.

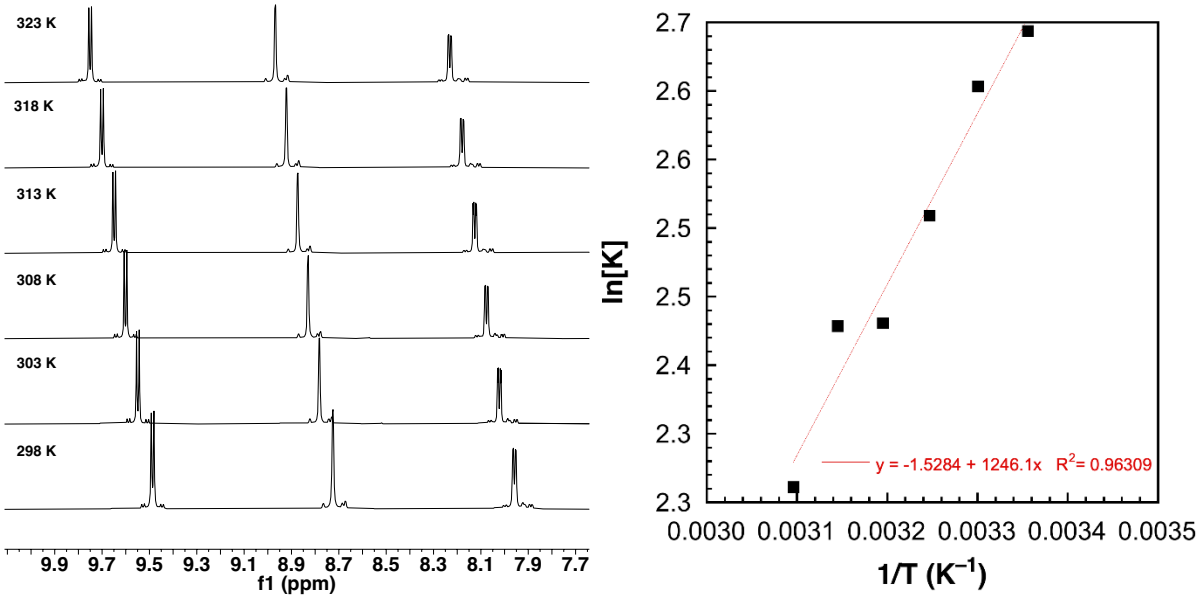

Figure S25. (*left*) ^{1}H NMR spectra of **2**|**Br** at various temperatures (right) Van't Hoff plot constructed using the VT NMR data from the equilibrium concentrations of **2** and **2-H$_2$O$^+$** at various temperatures.

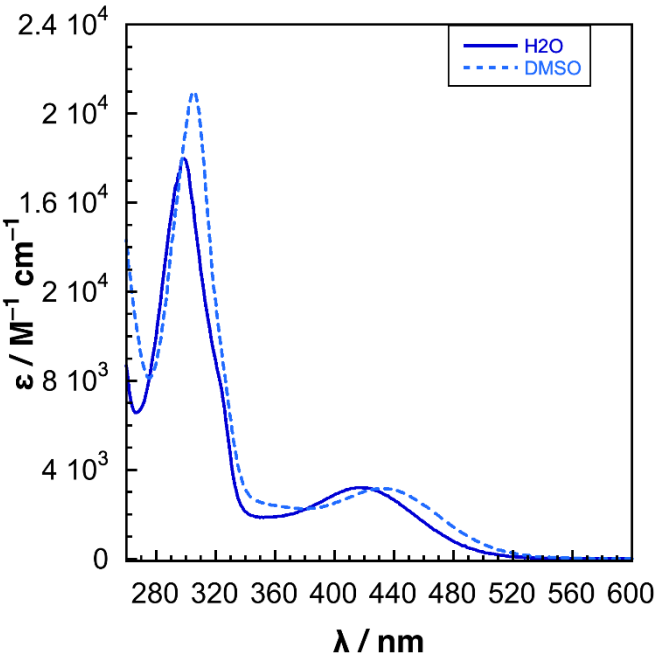

Figure S26. UV-vis spectra of **2|Cl** in H_2O and DMSO. Molar absorptivity of each complex was calculated from a linear fit derived from absorbance spectra of the complex at 5 different concentrations.

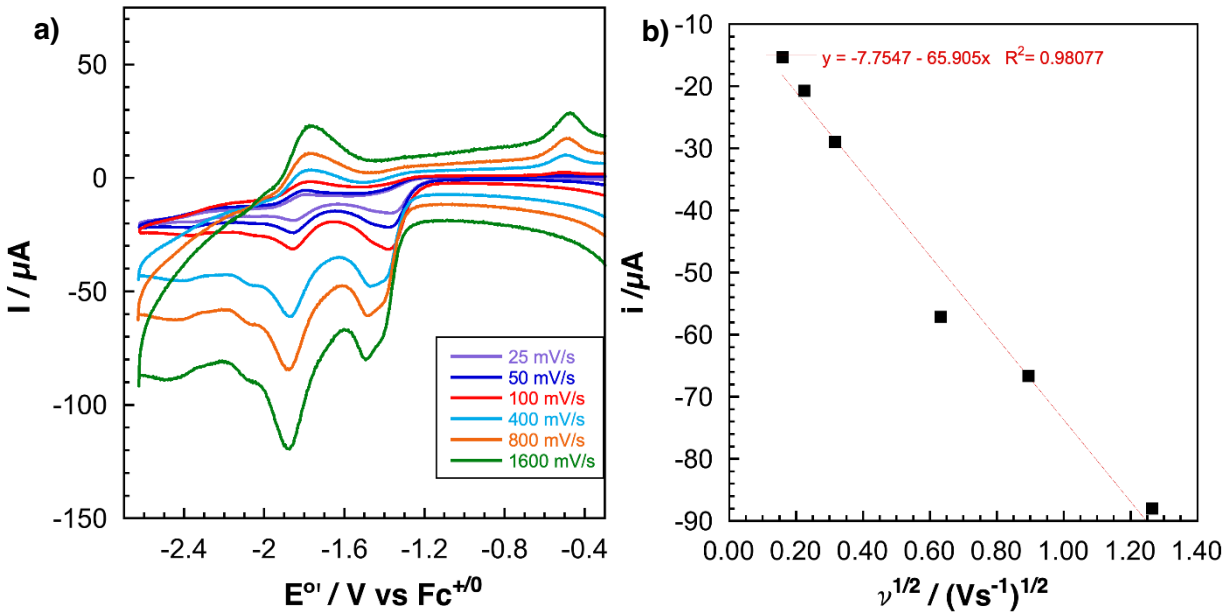

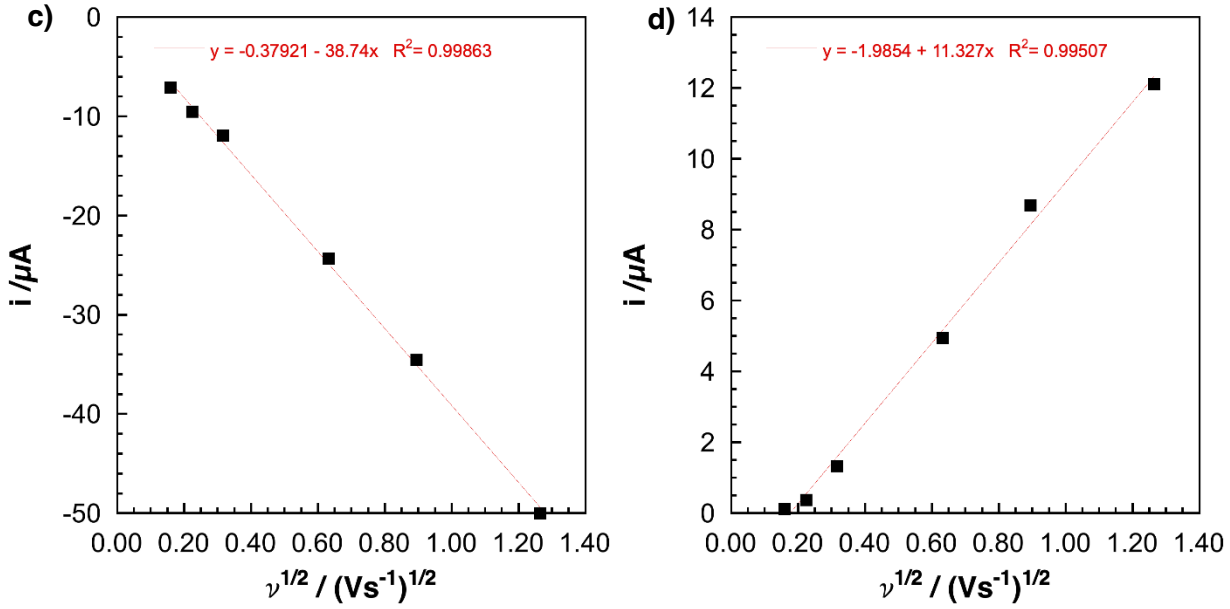

Figure S27. a) CVs of **1**|$\mathbf{PF_6}$ (1 mM) in N_2 sparged MeCN with 0.1 M $TBAPF_6$ supporting electrolyte at various scan rates. **b)** Randles-Sevcik plot for the first cathodic peak at –1.38 V vs $Fc^{+/0}$ **c)** Randles-Sevcik plot for the second cathodic peak at –1.86 V vs $Fc^{+/0}$ **d**) Randles-Sevcik plot for the dimer oxidation peak at –0.50 V vs $Fc^{+/0}$ **Figures 27b)-27d)** show that the observed current for each peak is linear with respect to $\nu^{1/2}$ indicating that **1**|$\mathbf{PF_6}$ is a freely diffusing species during the first voltage sweep.

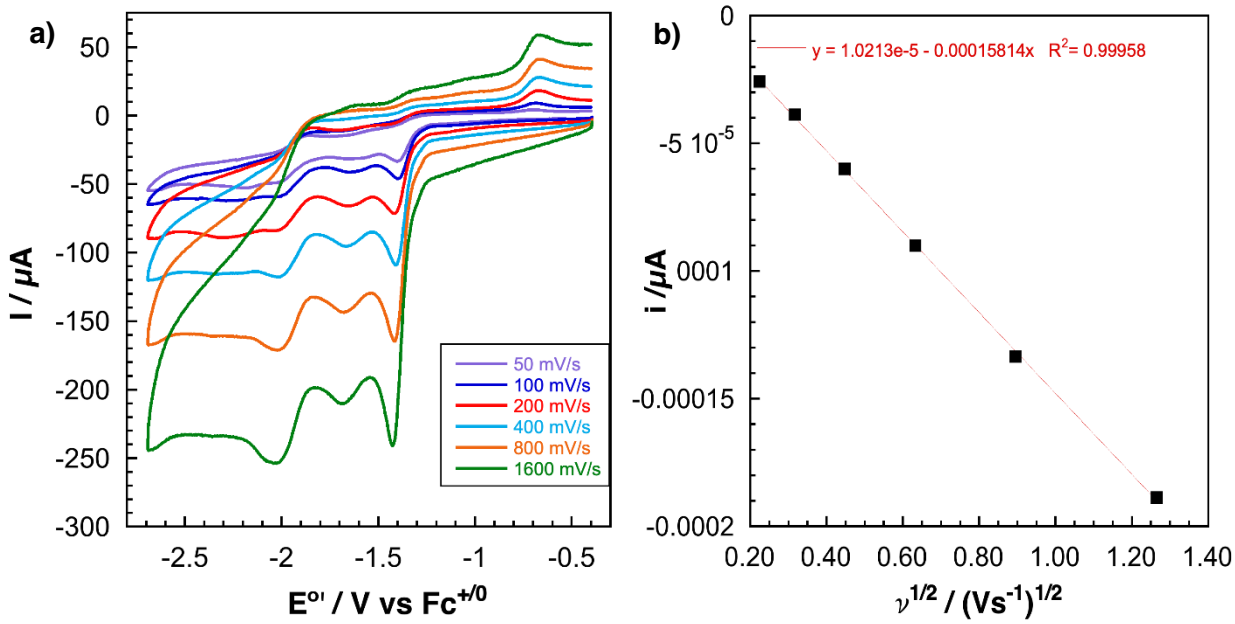

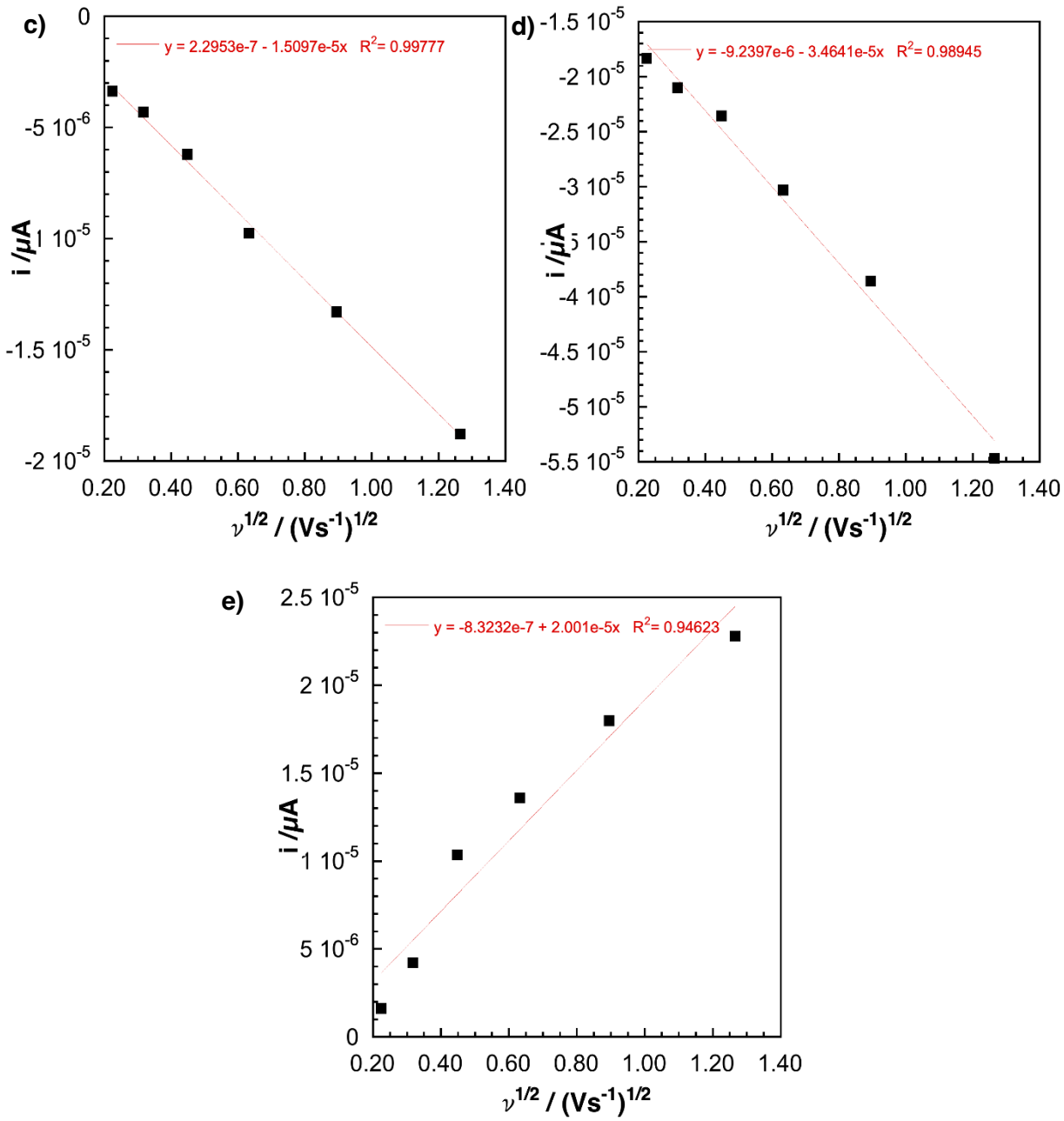

Figure S28. a) CVs of **2**|PF_6 (1mM) in N_2 sparged MeCN with 0.1 M $TBAPF_6$ supporting electrolyte at various scan rates. **b)** Randles-Sevcik plot for the first cathodic peak at –1.40 V vs $Fc^{+/0}$ **c)** Randles-Sevcik plot for the second cathodic peak at –1.66 V vs $Fc^{+/0}$ **d)** Randles-Sevcik plot for the third cathodic peak at –1.92 V vs $Fc^{+/0}$ **e**) Randles-Sevcik plot for the dimer oxidation peak at –0.69 V vs $Fc^{+/0}$ **Figures 28b)-27e)** show that the observed current for each peak is linear with respect to $\nu^{1/2}$ indicating that **2**|PF_6 is a freely diffusing species during the first voltage sweep.

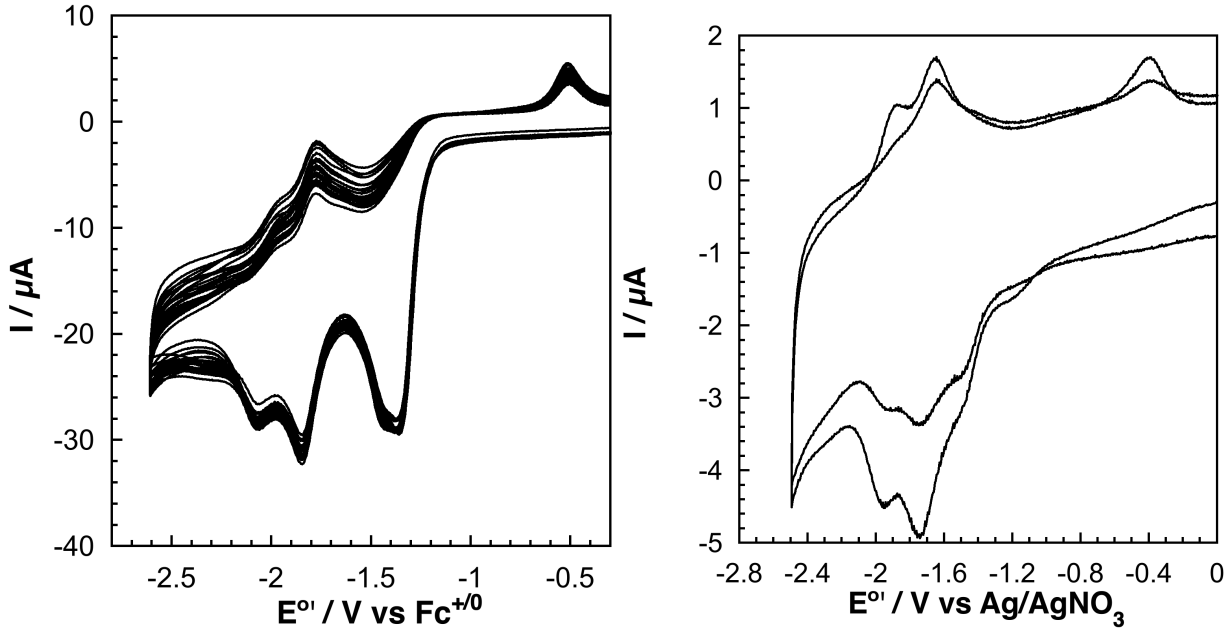

Figure S29. (*left*) 50-cycle CV experiment with **1**|**PF$_6$** (1 mM) in N_2 sparged MeCN with 0.1 M $TBAPF_6$ supporting electrolyte at 100 mV/s and (*right*) CV of MeCN rinsed electrode following the 50 cycle experiment in N_2 sparged 0.1 M $TBAPF_6$ electrolyte solution showing the presence of adsorbed complex. The decreased current observed in the second scan indicates that adsorbed species readily desorbs from the electrode with reductive cycling.

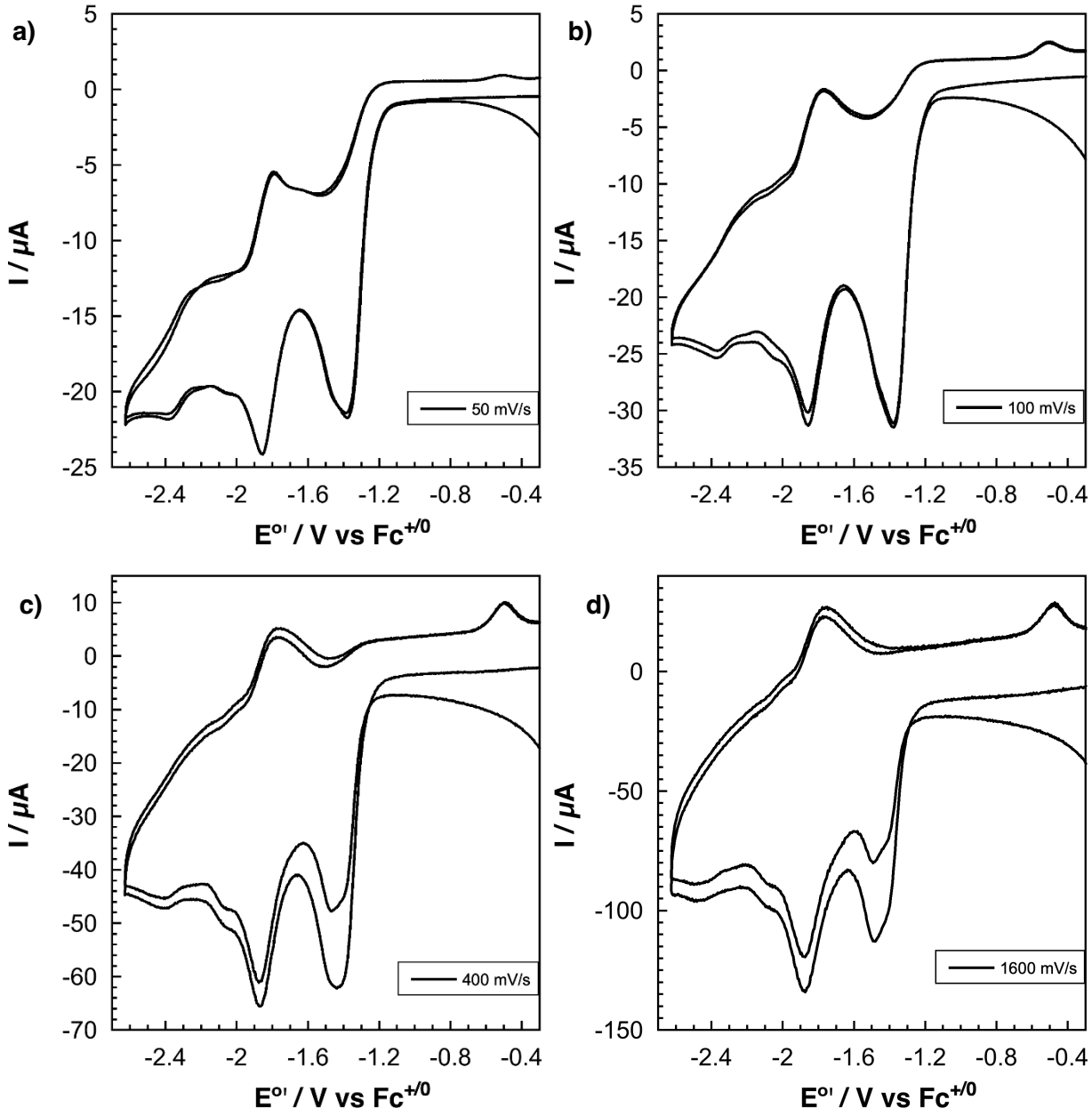

Figure S30. Cyclic voltammograms of **1|PF$_6$** (1 mM) in N_2 sparged 0.1 M $TBAPF_6$ MeCN electrolyte solution at **a)** 50, **b)** 100, **c)** 400, and **d)** 1600 mV/s showing the decrease in current observed for the peak at – 1.38 V vs $Fc^{+/0}$ in the second voltage sweep at higher scan rates.

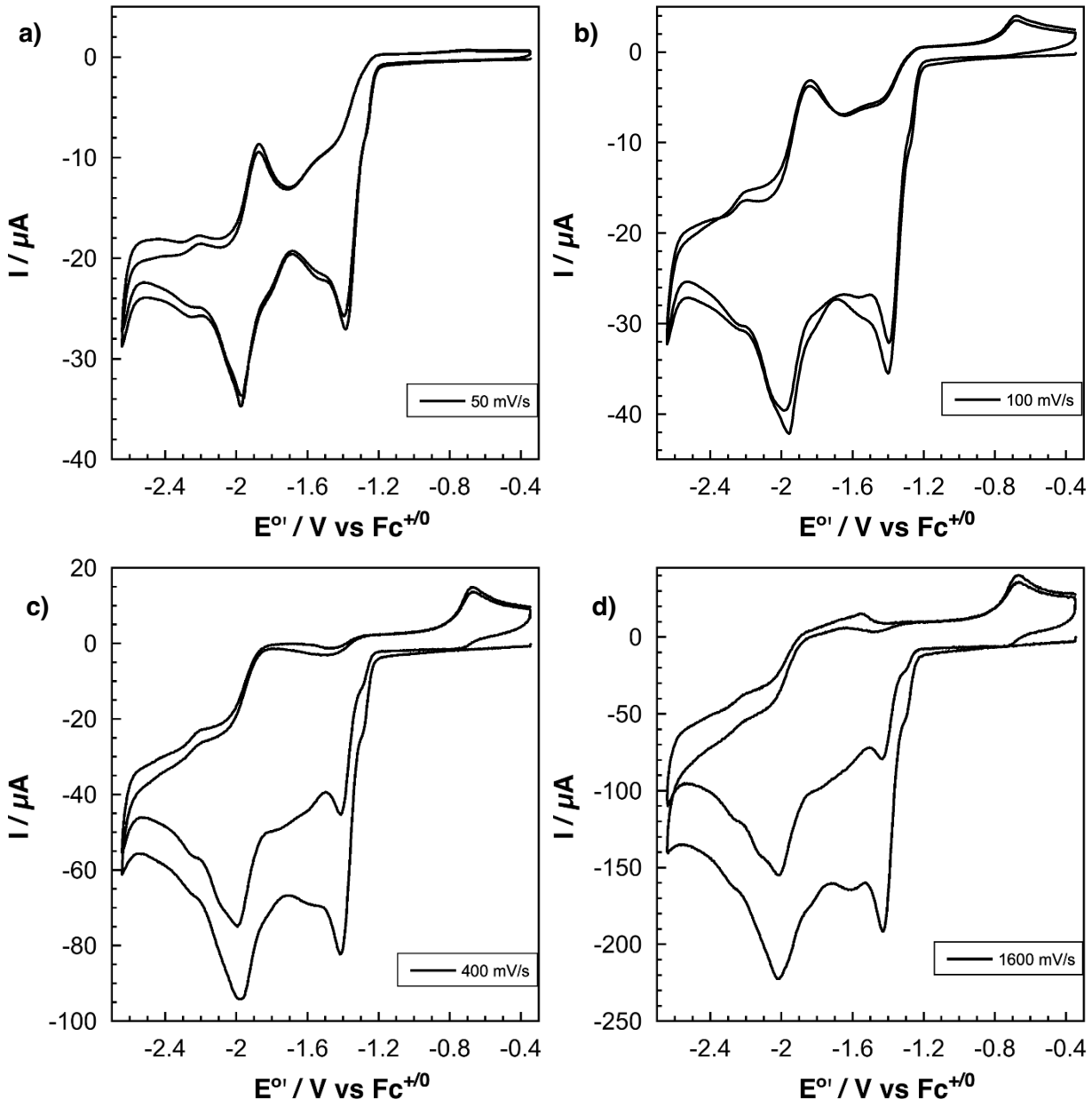

Figure S31. Cyclic voltammograms of **2**|PF_6 (1 mM) in 0.1 M $TBAPF_6$ MeCN electrolyte solution at **a)** 50, **b)** 100, **c)** 400, and **d)** 1600 mV/s showing the decrease in current observed for the peak at – 1.40 V vs $Fc^{+/0}$ in the second voltage sweep at higher scan rates.

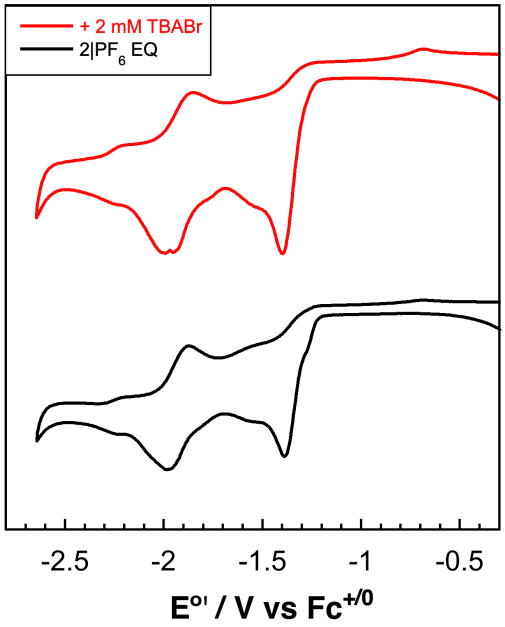

Figure S32. Cyclic voltammograms of $2|PF_6$ (1 mM) in N_2 sparged MeCN with 0.1 M $TBAPF_6$ supporting electrolyte at equilibrium (*black, bottom*) and at equilibrium with 2 mM TBABr (*red, top*) showing the lack of a shoulder attributed to **2-MeCN**$^+$ at –1.27 V vs $Fc^{+/0}$ with TBABr.

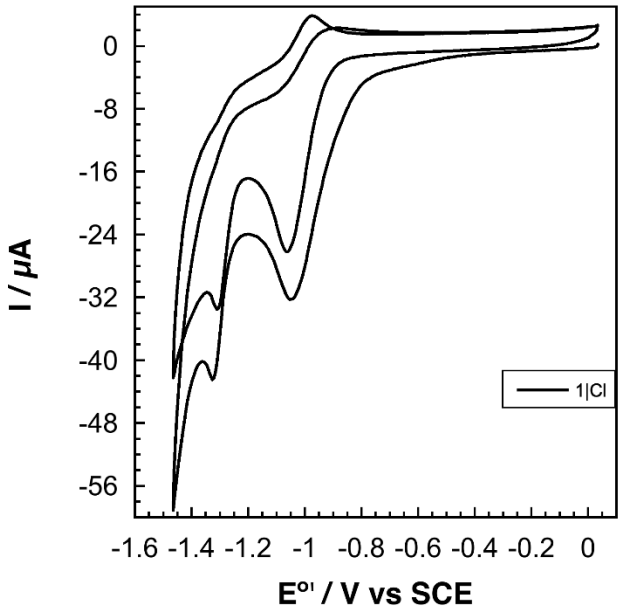

Figure S33. Cyclic voltammogram of **1|Cl** (1 mM) in N_2-purged 0.1 M $NaClO_4$ aqueous electrolyte solution obtained at 100 mV/s showing the loss of peak current from the first reduction in the second voltage sweep.

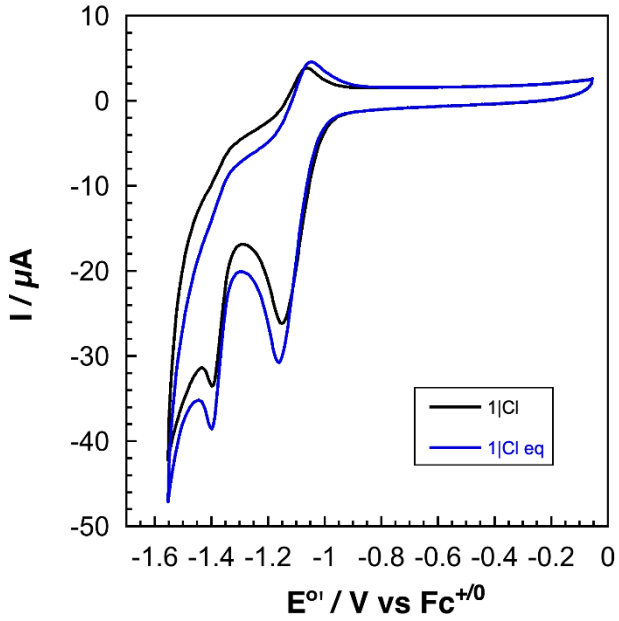

Figure S34. Cyclic voltammogram of **1|Cl** (1 mM) in N_2-purged 0.1 M $NaClO_4$ aqueous electrolyte solution obtained at 100 mV/s showing a freshly prepared solution of **1|Cl** (black), and a solution that had been allowed to equilibrate in solution for 1 d (blue).

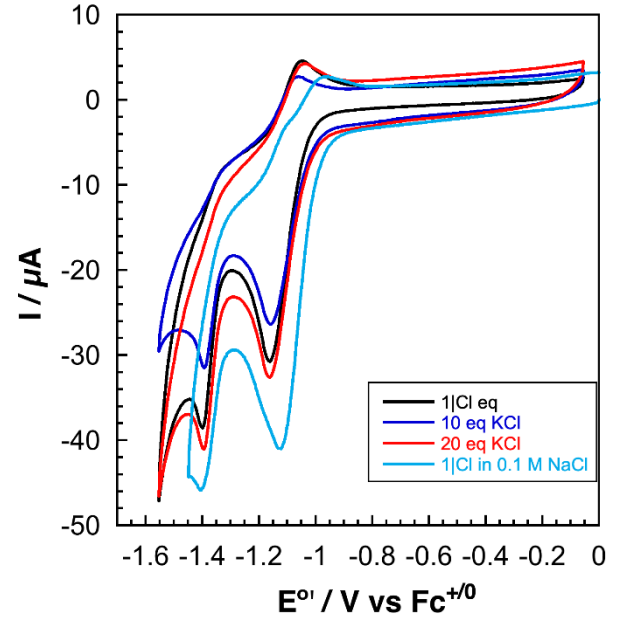

Figure S35. Cyclic voltammogram of **1|Cl** (1 mM) in N_2-purged 0.1 M $NaClO_4$ aqueous electrolyte solution with 0 (black), 10 (blue), and 20 mM (red) added KCl, and in N_2-purged 0.1 NaCl electrolyte solution (light blue). Voltammograms were collected using a scan rate of 100 mV/s.

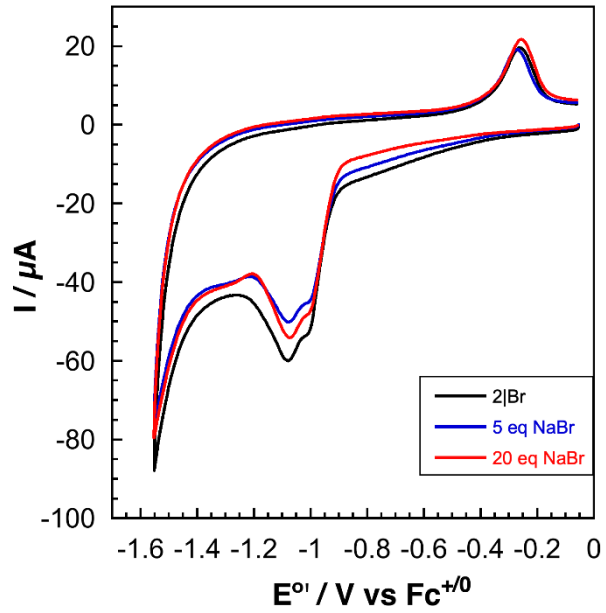

Figure S36. Cyclic voltammogram of **2|Br** (1 mM) in N_2-purged 0.1 M $NaClO_4$ aqueous electrolyte solution with 0 (black), 5 (blue), and 20 mM (red) added NaBr. Voltammograms were collected using a scan rate of 100 mV/s.

References

1) Fulmer, G. R.; Miller, A. J. M.; Sherden, N. H.; Gottlieb, H. E.; Nudelman, A.; Stoltz, B. M.; Bercaw, J. E.; Goldberg, K. I. NMR Chemical Shifts of Trace Impurities: Common Laboratory Solvents, Organics, and Gases in Deuterated Solvents Relevant to the Organometallic Chemist. *Organometallics* **2010**, *29*, 2176-2179
2) Swords, W. B.; Li, G.; Meyer, G. J. Iodide Ion Pairing with Highly Charged Ruthenium Polypyridyl Cations in CH3CN. *Inorg. Chem.* **2015**, *54* (9), 4512–4519.
3) Chen, S.-N.; Wu, W.-Y.; Tsai, F.-Y. Hiyama Reaction of Aryl Bromides with Arylsiloxanes Catalyzed by a Reusable Palladium(II)/Cationic Bipyridyl System in Water. *Tetrahedron* **2008**, *64* (35), 8164–8168.
4) Li, J.-H.; Wang, J.-T.; Hu, P.; Zhang, L.-Y.; Chen, Z.-N.; Mao, Z.-W.; Ji, L.-N. Synthesis, Structure and Nuclease Activity of Copper Complexes of Disubstituted 2,2′-Bipyridine Ligands Bearing Ammonium Groups. *Polyhedron* **2008**, *27* (7), 1898–1904.

5) Sheldrick, G. M. *Acta Cryst.* **1990**, A46, 467-473.
6) Sheldrick, G. M. *Acta Cryst.* **2015**, C71, 3-8.
7) Müller, P. *Crystallography Reviews* **2009**, *15*, 57-83.